Research Square

Preprints are preliminary reports that have not undergone peer review.
They should not be considered conclusive, used to inform clinical practice,
or referenced by the media as validated information.

Targeting trimeric SOD1 with Amisodin mitigates TDP-43-associated ALS pathology

Bum-Joon Park

b.jpark1219@pusan.ac.kr

Pusan National University/Rare Disease R&D Center, PRG S&T Co., Ltd https://orcid.org/0000-0002-6037-7219

Jin Han

Pusan National University https://orcid.org/0009-0000-4934-630X

Tae-Gyun Woo

Rare Disease R&D Center, PRG S&T Co., Ltd https://orcid.org/0000-0002-6957-0998

Yeon-Seon Mun

Rare Disease R&D Center, PRG S&T Co., Ltd

Hee Jeong Kim

Rare Disease R&D Center, PRG S&T Co., Ltd

Soyoung Park

Rare Disease R&D Center, PRG S&T Co., Ltd

So-mi Kang

Rare Disease R&D Center, PRG S&T Co., Ltd

Mua Lee

Pusan National University

Byung-Su Hong

Pusan National University

Jeongmo Kim

Pusan National University

Hyewon Jang

Seoul National University

Yun-Jeong Shin

Seoul National University

Yonghoon Kwon

Seoul National University

Bae-Hoon Kim

Pusan National University/PRG S&Tech https://orcid.org/0000-0001-6866-7248

Article

Keywords:

Posted Date: November 16th, 2026

DOI: https://doi.org/10.21203/rs.3.rs-11367184/v1

License: This work is licensed under a Creative Commons Attribution 4.0 International License.
Read Full License

Additional Declarations: There is **NO** Competing Interest.

Targeting trimeric SOD1 with Amisodin mitigates TDP-43-associated ALS pathology

Abstract

Amyotrophic lateral sclerosis (ALS) is a fatal neurodegenerative disorder characterized by progressive motor neuron loss. Although TDP-43 and SOD1 aggregation are major molecular features of ALS, their mechanistic relationship remains unclear. Here, we show that cytoplasmic TDP-43 induced by overexpression or cellular stress promotes SOD1 aggregation and preferentially interacts with trimer-associated SOD1 species. Destabilization of trimeric SOD1 disrupts the SOD1–TDP-43 interaction and reduces TDP-43 aggregation. Genetic depletion of SOD1 ameliorated motor dysfunction and neuronal loss in hTDP-43(+/+) mice, supporting a functional contribution of SOD1 to TDP-43 neurotoxicity. Pharmacological targeting of trimeric SOD1 with Amisodin reduced cytoplasmic TDP-43 accumulation, preserved neurons, improved motor function, and prolonged survival. Amisodin also reduced insoluble SOD1 and TDP-43 and their association in spinal cord tissue. These findings identify trimer-associated SOD1 as a functional modulator of TDP-43 proteotoxicity and support its selective targeting as a therapeutically actionable strategy for molecularly defined forms of TDP-43-associated ALS.

Background

Amyotrophic lateral sclerosis (ALS) is a relentlessly progressive neurodegenerative disorder characterized by loss of motor neuron, leading to muscle weakness, spasticity, and respiratory failure, with death occurring within two to five years after symptom onset [1-4]. Despite extensive research efforts over several decades, no therapeutic intervention has yet succeeded in stopping or reversing disease progression, largely due to an incomplete understanding of its molecular pathogenesis [5-7]. Clinically, ALS exhibits marked heterogeneity in age at onset, initial symptom site, and disease course, which complicates early diagnosis and prognostic prediction [1, 8]. Like other neurodegenerative diseases, abnormal protein aggregation is considered a central event in ALS pathogenesis. Approximately 90% of ALS cases are sporadic with no identifiable genetic cause; nevertheless, accumulating evidence supports aberrant protein aggregation as a convergent pathogenic mechanism [9, 10].

TAR DNA-binding protein 43 (TDP-43) is a predominantly nuclear RNA-binding protein, and its

cytoplasmic mislocalization and aggregation represent a defining pathological hallmark in the majority of ALS cases [11, 12]. In contrast, superoxide dismutase 1 (SOD1) is a ubiquitously expressed antioxidant enzyme, and its mutant or misfolded forms are well-established drivers of motor neuron degeneration in both familial and sporadic ALS [13, 14]. It remains unresolved whether TDP-43 pathology arises primarily from a toxic gain-of-function mechanism, a loss of its essential nuclear roles, or a combination of both [15-17]. Notably, wild-type SOD1 has been observed to colocalize with TDP-43 aggregates in numerous sporadic ALS cases, suggesting that SOD1 misfolding and aggregation may constitute a convergent pathogenic mechanism shared across both familial and sporadic forms of the disease [18, 19]. Also, several studies have suggested that these two proteins may influence each other's pathogenic behaviors [18, 20-23]. Nevertheless, the precise biological significance of SOD1 misfolding remains poorly understood [9, 10, 15, 24-27].

We previously demonstrated that overexpression-induced mislocalization of TDP-43 was found to enhance WT-SOD1 aggregation [28, 29]. We highlighted the trimeric SOD1 inhibitor and its inhibition of TDP-43 mislocalization, positioning PRG-A-04 as a strong drug candidate for ALS treatment [29]. In this report, we demonstrate that direct interaction between TDP-43 and trimeric SOD1 promotes the aggregation of both proteins, and that genetic ablation of SOD1 attenuates TDP-43-induced pathological phenotypes in vivo. This interdependence implies that TDP-43-mediated neurotoxicity depends on specific conformational states of endogenous SOD1, providing a mechanistic link between protein misfolding and sporadic ALS. Building upon this model, we investigated Amisodin (new candidate drug name of PRG-A-04), a selective inhibitor of trimeric SOD1, which effectively prevented cytoplasmic mislocalization of TDP-43 and ameliorated disease manifestations in both TDP-43 and SOD1 transgenic ALS models. Collectively, these findings identify pathogenic trimeric SOD1 conformers as key modulators of TDP-43-associated proteotoxicity and support selective inhibition of trimeric SOD1 as a promising therapeutic strategy molecularly defined subsets of sporadic ALS.

Results

Mislocalized cytoplasmic TDP-43 promotes aberrant aggregation of WT-SOD1 in neuronal cell

Approximately 97% of ALS patients show pathological abnormalities in TDP-43 [11, 32]. In our previous work, we demonstrated that increasing TDP-43 expression drives its mislocalization to the cytoplasm [28, 29]. Consistent with this, we confirmed that TDP-43 overexpression promotes key sALS-associated features, including the formation of cytoplasmic aggregates containing both TDP-43 and wild-type SOD1 (Fig. 1A, B, S1A). In addition, using the misfolded-SOD1-specific antibody (B8H10), we demonstrated that TDP-43 overexpression increased the formation of WT-SOD1 inclusions (Fig. 1C, D). The B8H10 clone has been reported to recognize various conformers of misfolded SOD1, whereas C4F6 has been reported to preferentially recognize a trimer-associated SOD1 conformation [31, 33]. Although B8H10 is not a trimer-specific antibody, we found that it preferentially recognized the trimer-enriched SOD1 species under our experimental conditions (Fig. S1B, C).

Cellular stressors such as CoCl2 (hypoxia mimetic) or TPEN (Zn^{2+} chelator) elicited abnormal cytoplasmic localization and inclusion of TDP-43, concomitant with WT-SOD1 inclusion (Fig. 1E-G, S1D-F). cellular stress induced B8H10- and C4F6-reactive SOD1 oligomeric species that were associated with TDP-43 (Fig. S1G). These findings are consistent with the presence of trimer-associated or trimer-like SOD1 conformations within heterogenous SOD1 oligomeric species associated with TDP-43. Notably, stress-induced SOD1 oligomerization was abolished by TDP-43 suppression (Fig. 1H), indicating that TDP-43 is required for this pathological process. Together, these results suggested that cellular stress promotes cytoplasmic mislocalization of TDP-43, which in turn facilitates aberrant aggregation of WT-SOD1.

To assess whether these phenomena occur in an in vivo context, we examined hTDP-43 transgenic mice, a model that recapitulates key pathological features of sporadic ALS [34, 35]. Homozygous hTDP-43 mice exhibited an abnormal hindlimb clasping response, characterized by flexion of the hindlimbs toward the torso during tail suspension, whereas non-transgenic littermates displayed normal hindlimb extension (Fig. 1I, S1H). This aberrant reflex is recognized as an early indicator of impaired motor function in several ALS mouse models. In addition, hTDP-43 (+/+) mice displayed progressive body weight loss and a significant reduction in brain size compared with wild-type (non-transgenic) and heterozygous hTDP-43 (+/-) littermates (Fig. S1I-K).

Consistent with our cellular findings, spinal motor neurons of hTDP-43-overexpressing mice showed pronounced cytoplasmic mislocalization of TDP-43 (Fig. 1I, J). Notably, these mice also exhibited WT-SOD1 inclusions, suggesting that pathological TDP-43 overexpression promotes abnormal accumulation of endogenous mouse SOD1 in vivo (Fig. 1K). To further examine WT-SOD1 accumulation using an independent biochemical approach, we performed soluble/insoluble fractionation of spinal cord lysates. This analysis revealed increased levels of endogenous mouse SOD1 in the insoluble fraction of hTDP-43-overexpressing mice compared with control mice (Fig. 1L), providing biochemical evidence for enhanced SOD1 insolubility in vivo. Furthermore, we observed an interaction between hTDP-43 and mouse SOD1, although this interaction was weaker than that observed with human SOD1 (Fig. S1L). This observation further support that hTDP-43-overexpressing mice closely reflect the pathological features observed in sALS patient tissues. Taken together, our findings indicate that cytoplasmic TDP-43, which can arise from either overexpression or cellular stress, increased SOD1 inclusion formation and insolubility as an important pathological consequence of TDP-43 mislocalization.

Given that neuronal vulnerability is a defining pathological feature of many neurodegenerative diseases, we hypothesized that cytoplasmic mislocalization of TDP-43 induced by its overexpression may occur in a cell type dependent manner. This phenotype was observed in spinal neurons from hTDP-43 WT-overexpressing mice (Fig. S2A, B). In addition, overexpression of TDP-43 across multiple cell lines, most prominently in neuronal cell lines, led to a pronounced redistribution of TDP-43 from the nucleus to the cytoplasm (Fig. S2C-E).

It has been reported that, in neurons, the nuclear membrane complex is structurally less rigid and depends on primarily on lamin B expression [36-38], potentially rendering it more vulnerable to perturbations in nucleocytoplasmic transport. It is presumed that increased TDP-43 levels promote leakage or dysregulated export into the cytoplasm by compromising nuclear envelope integrity. Consistent with this notion, we observed that susceptibility to TDP-43 mislocalization correlated with reduced expression of lamin proteins, suggesting that compromised nuclear envelope integrity may facilitate aberrant cytoplasmic accumulation of TDP-43 (Fig. S2F). Supporting this hypothesis, ectopic

expression of lamin A or lamin C, conditions resembling those of non-neuronal cells, markedly reduced cytoplasmic TDP-43 levels following its overexpression in neuronal cells (Fig. S2G, H). Conversely, knockdown of lamin A/C, which mimics the lamin composition of neuronal cells, promoted cytoplasmic mislocalization of TDP-43 by its overexpression in non-neuronal cell types (Fig. S2I, J). Although these findings implicate nuclear envelope instability as a contributing factor, the precise molecular mechanisms that drive this neuron-selective mislocalization of TDP-43 remain to be fully elucidated.

SOD1 depletion attenuates TDP-43 aggregation and cytoplasmic mislocalization

Although several studies have suggested pathogenic crosstalk between TDP-43 and SOD1, their biochemical relationship remains incompletely defined. To determine whether SOD1 aggregation is dependent on TDP-43, we first examined the interaction between these two proteins in vivo. Notably, double heterozygous hTDP-43 (+/-);hSOD1-G93A (+/-) transgenic mice did not exhibit exacerbated disease phenotypes relative to hSOD1-G93A (+/-) mice (Fig. S3A, B). This observation indicated that TDP-43 does not potentiate mutant SOD1-driven pathological aggregation, even under conditions of increased TDP-43 expression. Consistently, TDP-43 overexpression did not accelerate SOD1 inclusion induced by ectopic SOD1-G93A expression (Fig. S3C, D). Although TDP-43 suppression markedly reduced WT-SOD1 aggregation triggered by Zn^{2+} chelation (Fig. 1H), aggregation driven by the ALS-associated SOD1-G93A mutation or the trimer-stabilizing SOD1-G147P variant was unaffected by TDP-43 downregulation (Fig. S3E-H). These results indicate that mutant SOD1 aggregation proceeds independently of TDP-43.

We next assessed whether SOD1 contributes to TDP-43 aggregation. Interestingly, SOD1 knockdown markedly attenuated TDP-43 inclusion and cytoplasmic mislocalization induced by TDP-43 overexpression and cellular stresses (Fig. 2A, B, D, E, S4A). Consistently, TDP-43 oligomerization induced under the same conditions was also reduced (Fig. 2C, F, S4B), indicating that SOD1 facilitates cytoplasmic TDP-43 aggregation. To determine whether this process requires cytosolic interaction between the two proteins, we inhibited TDP-43 nuclear export using the nuclear export inhibitor, Leptomycin B (LMB). LMB treatment modestly reduced the cytoplasmic accumulation of TDP-43 (Fig.

2G, H, S4C, D) and suppressed oligomerization of TDP-43 (Fig. 2I, J, S4E). Together with the pronounced suppression of aggregation observed following SOD1 knockdown, these findings suggest that cytoplasmic localization of TDP-43 facilitates SOD1-dependent pathological TDP-43 assembly. To further validate the effect of SOD1 depletion on TDP-43 pathology, we performed complementary experiments using HEK293T SOD1-knockout cells. Consistent with the knockdown results, SOD1 deficiency attenuated cytoplasmic TDP-43 mislocalization and reduced insoluble TDP-43 levels (Fig. 2K-M). Collectively, these findings support a model in which SOD1 acts as a functional modifier of cytoplasmic TDP-43 mislocalization, aggregation, and oligomerization under pathological conditions.

Interaction of TDP-43 with trimer-associated SOD1 promotes reciprocal protein aggregation

To determine whether specific conformational states of SOD1 influence its interaction with TDP-43 under pathological conditions, we examined the binding affinity between these proteins in cellular models. In cells, MT-SOD1 (G85R and G93A) bound more strongly to TDP-43 than WT-SOD1 (Fig. S5A). Consistent with this observation, assays using purified recombinant proteins provided direct evidence that TDP-43 physically binds to SOD1 (Fig. 3A).

In our previous report, we showed that SOD1 aggregation is initiated through formation of trimeric SOD1 species [29]. Based on this finding, we hypothesized that TDP-43 preferentially recognizes the trimeric conformation of SOD1, thereby promoting the formation of higher-order aggregation complexes. Using the SOD1 trimer-stabilizing recombinant protein (SOD1-G147P), we observed a markedly enhanced interaction with TDP-43 compared with WT-SOD1 (Fig. 3B, S5B). To test whether this interaction depends on trimer-associated SOD1 conformations, we examined trimer-destabilizing SOD1-N53I and SOD1-D101I variants. Both variants markedly reduced the enhanced interaction between mutant SOD1 and TDP-43 (Fig. 3C). Functionally, expression of the trimer-destabilizing SOD1 mutants markedly reduced TDP-43 inclusion formation and insolubility induced by cytoplasmic TDP-43 overexpression (Fig. 3D-F). Moreover, oligomerization of both SOD1 and TDP-43 induced by TDP-43 overexpression or cellular stress was effectively suppressed in the presence of the trimer-destabilizing SOD1 mutants (Fig. 3G, S5C).

We next mapped the TDP-43 region responsible for SOD1 binding. His-SOD1 pull-down assay identified the RNA recognition motif (RRM; residues 102-269) as the core region mediating SOD1 binding (Fig. 3H, I). Because the RRM region physiologically binds RNA, we considered the possibility that the observed SOD1-TDP-43 association might be mediated indirectly through RNA bridging. To address this possibility, we performed an interaction assay using recombinant WT-SOD1 incubated with RNase- or RNase inhibitor-treated lysates expressing TDP-43 domain fragments. The interaction between SOD1 and the TDP-43 RRM-containing region was maintained following RNase treatment (Fig. S5D), suggesting that the interaction is not primarily dependent on RNA-mediated bridging. Consistent with these biochemical findings, protein–protein docking predicted a plausible interface between trimeric SOD1 and the TDP-43 RRM domain (Fig. 3J, S5E), and the RRM domain showed a higher predicted binding affinity for trimeric SOD1 than for monomeric or dimeric SOD1 (Fig. S5F). These results provide structural support for the feasibility of this interaction.

Based on these findings, we propose that aberrantly accumulated cytoplasmic TDP-43 interacts with specific SOD1 conformations through its RRM-containing region, promoting reciprocal protein misfolding. In particular, trimer-associated SOD1 conformations may facilitate this pathogenic cross-talk, providing a mechanistic framework for how non-mutational proteotoxicity could contribute to pathogenic cascades in sALS.

SOD1 knockout attenuates TDP-43-associated pathology in hTDP-43 transgenic mice

Given our results demonstrating that SOD1 contributes to TDP-43 aggregation (Fig. 2), we hypothesized that genetic ablation of SOD1 would ameliorate the pathological phenotypes in the hTDP-43 (+/+) mice. To test this, we generated double-heterozygous hTDP-43 (+/-);mSOD1 (+/-) mice to generate hTDP-43 (+/+);mSOD1 (-/-) offspring (Fig. 4A). The hTDP-43 (+/+) line is an aggressive disease model characterized by early-onset muscle paralysis emerging around postnatal day 18 and an extremely short lifespan of approximately 21-25 days (Fig. 4B). Although no clear recovery in body weight was observed, the severe motor deficits seen in hTDP-43 (+/+) mice were interestingly delayed in hTDP-43 (+/+);mSOD1 (-/-) mice (Fig. 4C, D). Representative behaviors recorded in the open-field

test are shown in Supplementary video [see Additional file 1]. Motor improvement in the hTDP-43 (+/+);mSOD1 (-/-) compound mice was further supported by reduced levels of neurofilament light chain (NF-L, a biomarker of neuronal injury) in peripheral blood, indicating enhanced neuronal preservation upon SOD1 suppression (Fig. 4E). Consistent with these functional improvements, histological analysis of spinal cord revealed that the loss of NeuN-positive neurons observed in hTDP-43 (+/+) mice was significantly restored in a mouse with concurrent SOD1 deficiency (Fig. 4F, G, S6A, B). Notably, TDP-43 mislocalization was reduced in the hTDP-43 (+/+);mSOD1 (-/-) mice without substantial change in total TDP-43 expression (Fig. 4H-K, S6C-E). Furthermore, the nuclear portion of TDP-43 slightly increased in hTDP-43 (+/+);mSOD1 (-/-) mice (Fig. 4I), suggesting that SOD1 suppression effectively alleviates cytoplasmic mislocalization, thereby promoting the proper nuclear retention of TDP-43.

Despite these improvements in motor function and TDP-43 homeostasis, only a modest extension of lifespan, approximately 5 days, was observed in a subset of hTDP-43 (+/+);mSOD1 (-/-) mice (Fig. 4L). This limited effect on overall survival may reflect the persistence of severe neurodevelopmental abnormalities, particularly the pronounced neuronal loss in the hippocampal CA3 region of hTDP-43 (+/+) mice, which was not fully rescued by SOD1 deficiency (Fig. S6F-H). The CA3 region has been reported to be selectively vulnerable in several models of TDP-43-related neurodegeneration, and severe hippocampal pathology has been associated with postnatal mortality [39, 40]. In contrast, SOD1 aggregation is rarely observed in the hippocampus [41, 42]. raising the possibility that this component of the phenotype is relatively independent of SOD1. Thus, although SOD1 deficiency substantially preserved spinal neurons, persistent hippocampal pathology may have constrained the overall survival benefit. In addition, complete SOD1 ablation is biologically distinct from selective targeting of pathogenic SOD1 conformers, because it removes both toxic SOD1 species and physiological SOD1 functions. This distinction may partly explain why conformer-selective pharmacological intervention can produce therapeutic effects that are not fully recapitulated by constitutive SOD1 deletion.

Amisodin disrupts SOD1-TDP-43 proteotoxicity and reduces TDP-43 aggregation

In our previous study, we identified PRG-A-04 (renamed as Amisodin), as a trimer-targeting SOD1

inhibitor with therapeutic activity against SOD1 aggregation [29]. Consistent with the importance of trimer-associated SOD1 conformations, we found that the trimer-destabilizing SOD1-N53I and SOD1-D101I variants reduced insoluble TDP-43 accumulation and TDP-43 oligomerization (Fig. 3D-F). These findings prompted us to test whether pharmacological targeting of trimeric SOD1 could also attenuate TDP-43 pathology. As expected from our previous work, Amisodin preserved motor function, reduced neuronal loss, and prolonged survival in hSOD1-G93A Tg mice (Fig. S7A-D). Furthermore, Amisodin showed the inhibitory effect on the TDP-43 aggregation by its overexpressed conditions in several cell lines (Fig. 5A, B). Furthermore, Amisodin suppressed the interaction between SOD1-G147P and TDP-43 (Fig. 5C), thereby reduced the oligomerization of SOD1 and TDP-43 (Fig. 5D, Fig. S7E). Notably, Amisodin inhibited SOD1 oligomerization but did not directly affect TDP-43 self-oligomerization induced by recombinant TDP-43 (Fig. 5E). Together, these findings support a model in which Amisodin attenuates TDP-43 pathology primarily through modulation of trimer-associated SOD1 states, thereby disrupting the reciprocal proteotoxic interaction between SOD1 and TDP-43.

Next, we evaluated the therapeutic efficacy of Amisodin using hTDP-43 (+/+) mice. Because the rapid disease onset of this model precludes direct postnatal drug treatment, we adopted a maternal administration strategy in which Amisodin was orally delivered to hTDP-43 (+/-) parent mice. In our previous study, we characterized the pharmacokinetic properties, BBB (Blood-Brain Barrier) permeability assessed by PAMPA (Parallel Artificial Membrane Permeability Assay), and brain exposure of Amisodin were reported. Amisodin showed moderate membrane permeability and substantial brain exposure, with a brain-to-plasma concentration ratio of 2.11. Amisodin also exhibited favorable bioavailability (~57%) in mice [29]. To assess maternal-to-offspring transfer and CNS exposure of Amisodin, parental mice were orally administered Amisodin three times per week beginning at mating. Following mating, Amisodin administration was continued in the female mice until postnatal day 18, resulting in a total treatment period of approximately 1 month (Fig. S8A). LC-MS/MS analysis of the offspring showed Amisodin at mean concentrations of 136 ng/mL in plasma, 277 ng/g in brain and 495 ng/g in spinal cord (Fig. S8B). These findings demonstrate that Amisodin administered to the parental mice is transferred to the offspring and reaches the brain and spinal cord, providing direct

evidence of systemic and CNS exposure in the offspring.

To evaluate the therapeutic efficacy of Amisodin in hTDP-43 (+/+) offspring, two independent treatment cohorts were established using hTDP-43 (+/-) parental mice. In the first cohorts, to ensure sustained drug exposure before and during gestation, Amisodin was administered orally to 6-month-old hTDP-43 (+/-) parental mice three times per week for approximately 1 month before mating and was continued in female mice throughout gestation (Fig. 5F). Remarkably, offspring from Amisodin-treated parents exhibited substantially ameliorated neuronal loss compared with those from vehicle-treated parents (Fig. 5G, H). This improvement was accompanied by a reduction in cytoplasmic TDP-43 mislocalization in hTDP-43(+/+) offspring (Fig. 5I, J).

In the second treatment cohorts, to evaluate the effects of prolonged maternal Amisodin administration, treatment was continued in female mice throughout pregnancy and following parturition until P21 of the offspring, at which point treatment was discontinued (Fig. S8C). hTDP-43 (+/+) offspring from Amisodin-treated hTDP-43 (+/-) parental mice improved motor function, reduced plasma NF-L level, and attenuated neuronal loss compared with offspring from vehicle-treated parents (Fig. S8D-H). Consistent with the findings from the first cohort, cytoplasmic TDP-43 mislocalization was also reduced (Fig. S8I, J). To assess the biochemical effect of Amisodin in vivo, we performed soluble/insoluble fractionation of spinal cord lysates. Accumulation of insoluble TDP-43 and mouse SOD1 was reduced in hTDP-43 (+/+) offspring from Amisodin-treated parents compared with those from vehicle-treated parents (Fig. 5K). In addition, the interaction between mSOD1 and TDP-43 was reduced in hTDP-43 (+/+) offspring from Amisodin-treated parents (Fig. S8K). Notably, the hTDP-43 (+/+) line represents an aggressive disease model characterized by early-onset motor paralysis and a markedly shortened lifespan of approximately 21–25 days. Despite the severity of this phenotype, Amisodin treatment extended survival by approximately 9.7 days (Fig. 5L), indicating a substantial therapeutic effect even in this rapidly progressive model.

We additionally examined whether Amisodin interacts with mouse SOD1. Streptavidin pull-down assays using biotinylated Amisodin demonstrated binding to both WT and mutant forms of mouse SOD1 (Fig. S9A). Moreover, the interaction between mouse SOD1-G93A and TDP-43 was reduced in

the presence of Amisodin (Fig. S9B). These experiments provide additional evidence that the effects of Amisodin observed in our mouse experimental system can involve mouse SOD1 directly. In addition, in silico docking analysis predicted a higher binding affinity of Amisodin for trimeric SOD1. Amisodin appears to occupy a pocket adjacent to, and partially overlapping with, the predicted TDP-43-binding surface on the SOD1 trimer. This raises the possibility that Amisodin disrupts SOD1-TDP-43 interaction by blocking the interface or stabilizing an SOD1 conformation that is less favorable for TDP-43 binding. These findings provide a structural support for a preferential interaction between Amisodin and trimeric SOD1 (Fig. S9C–E).

Together, these findings indicate that Amisodin mitigates TDP-43-associated pathology in vivo, accompanied by reduced accumulation of insoluble SOD1 and TDP-43 and decreased SOD1-TDP-43 association. Although sustained direct postnatal administration was not feasible in this aggressive model, maternal administration resulted in measurable CNS exposure in the offspring and produced significant therapeutic effects, supporting the potential of Amisodin as a candidate treatment for TDP-43-associated sALS.

Amisodin ameliorates TDP-43-associated pathology in hTDP-43 transgenic mice

Given the short lifespan of hTDP-43 (+/+) mice, which limits longitudinal evaluation of therapeutic efficacy, we next assessed the in vivo efficacy of Amisodin using the hTDP-43 (+/-) mice that recapitulates slower disease progression. Amisodin was orally administered (three times weekly) to 8-month-old hTDP-43 (+/-) mice to evaluate its in vivo efficacy, with treatment continued until 16 months of age (Fig. 6A). Throughout the administration period, no significant changes in body weight were observed (Fig. 6B), indicating that Amisodin is well tolerated and suitable for long-term administration without toxicity. Motor performance was subsequently evaluated using the vertical grid test and grip-strength assessment. Vehicle-treated hTDP-43 (+/-) mice displayed age-dependent motor decline, characterized by prolonged descent times, including impaired turning behavior, and reduced grip strength by 14 months of age. In contrast, Amisodin treatment significantly improved motor performance in vertical test and preserved grid strength (Fig. 6C, D). Consistent with these functional

improvements, plasma NF-L levels were reduced in a dose-dependent manner (Fig. 6E). Histological analysis of cervical spinal cord tissue at 16 months revealed that Amisodin treatment preserved NeuN and MAP2-positive neuronal populations compared with vehicle-treated controls (Fig. 6F-I). Furthermore, cytosolic mislocalization of TDP-43 was alleviated in Amisodin-treated hTDP-43(+/+) mice, accompanied by a modest increase in the nuclear portion of TDP-43 (Fig. 6J, K, S10A, B), indicating partial restoration of TDP-43 nuclear localization. Importantly, comparable therapeutic benefits, including preservation of motor performance and neuroprotective effects, were observed even when Amisodin treatment was initiated at a later stage, supporting both protective and disease-modifying properties of the compound (Fig. S10C-H). Together, these findings demonstrated that Amisodin, targeting for trimeric SOD1, represents a promising therapeutic candidate for TDP-43-related sALS, with efficacy under long-term administration and minimal toxicity.

Discussion

In this study, we show that increased TDP-43 expression or cellular stress promotes its aberrant redistribution to the cytoplasm (Fig.1), where it forms aggregates and engages trimeric SOD1 through its RNA recognition motif, thereby enhancing SOD1 oligomerization (Fig. 2). Conversely, disruption of trimeric SOD1 formation diminished the aggregation of both proteins, underscoring a reciprocal pathogenic axis (Fig. 2). Genetic experiments further corroborate this dependency: eliminating SOD1 markedly attenuated TDP-43-mediated pathological phenotypes (Fig. 3). Collectively, these findings demonstrate a functional interaction between TDP-43 and SOD1 and identify trimeric SOD1 as a modulator of TDP-43-associated proteotoxicity (Fig. 6L).

In recent years, therapeutic development in ALS has shifted from broadly neuroprotective approaches toward mechanism-based interventions targeting genetic drivers, proteinopathy, bioenergetic dysfunction, and neuroinflammation [43]. Nevertheless, clinical translation remains challenging because of substantial disease heterogeneity, modest treatment effect sizes, and the lack of robust biomarkers and responder-enrichment strategies [43, 44].

SOD1 is one of the most clinically advanced therapeutic targets in ALS. Tofersen has shown that

reducing SOD1 can favorably affect disease-associated biomarkers and may provide clinical benefit in selected patients with SOD1-ALS, although its long-term therapeutic impact remains under evaluation [45, 46]. Because native SOD1 also contributes to lysosomal and cellular homeostasis [47] sustained global suppression may carry biological liabilities. Selective targeting of pathogenic SOD1 conformers may therefore offer a strategy to retain physiological SOD1 function while suppressing toxic proteotoxic species.

Importantly, recent clinical and experimental findings suggest that SOD1-associated pathology may extend beyond genetically defined SOD1-ALS [48-50]. In the AP-101 Phase 2 study, favorable clinical signals were observed in sporadic ALS, including a benefit on the exploratory composite endpoint of death or ventilatory support, while a slower decline in ALSFRS-R scores was reported in patients with elevated baseline misfolded SOD1 [48, 51]. Although these findings require further validation, they support the possibility that a subset of sALS may exhibit therapeutically relevant SOD1 proteotoxicity.

TDP-43 pathology, meanwhile, represents a major molecular feature of sporadic ALS. Mislocalized and misfolded TDP-43 has been proposed to undergo prion-like templated propagation. Pathological TDP-43 species are transferred between neurons and glial cells and promote further protein misfolding, potentially contributing to the progressive and regionally expanding nature of the disease [52-54]. Rather than viewing sALS solely as an idiopathic clinical syndrome, accumulating molecular evidence increasingly supports TDP-43 dysfunction as a major biological axis of disease in most patients [55-57]. Beyond identifying TDP-43 pathology itself, however, understanding the molecular factors that modulate TDP-43-mediated neurotoxicity may reveal additional therapeutic targets.

Several lines of evidence support a mechanistic relationship between SOD1 and TDP-43 rather than two entirely independent pathological processes. Post-mortem spatial profiling shows that SOD1 and TDP-43 pathologies co-localize and covary within human spinal motor neurons, supporting mechanistic linkage rather than parallel, independent lesions [18]. Experimental systems demonstrate bidirectional cross-talk: mislocalized or overexpressed TDP-43 drives misfolding/aggregation of wild-type SOD1 and propagates SOD1 misfolding in a prion-like manner, whereas exogenous SOD1 aggregates reciprocally induce TDP-43 mislocalization and aggregation [20, 21]. Mechanistic dissection further

identifies aromatic and tryptophan residues at the TDP-43-SOD1 interface that facilitate cross-seeding, highlighting residue-level interactions as druggable nodes [22].

Growing mechanistic evidence implicates protein misfolding, especially formation of toxic SOD1 oligomers/trimers as an early driver of motor-neuron injury [33, 58, 59]. Building on this, we reported a first-generation inhibitor (PRG-A-01) that reduced SOD1 aggregation and improved survival in hSOD1-G93A mice, followed by an optimized trimer-targeting agent (PRG-A-04) with broader preclinical efficacy [28, 29]. Furthermore, trimer-focused SOD1 inhibitors attenuate TDP-43 oligomerization and cytoplasmic mislocalization, suggesting that disruption of pathogenic SOD1 intermediates may indirectly restore TDP-43 proteostasis [29]. These findings prompted us to examine the molecular basis of the interaction between trimeric SOD1 and TDP-43.

To explore a potential molecular basis for this interaction, we performed in silico structural modeling, which predicted an interface between the SOD1 trimer and the TDP-43 RRM domain. The predicted interface involved several specific residue pairs between SOD1 and TDP-43, including Glu133-Lys145, Asp52-Arg227, Thr54-Lys263, and Glu49-Asn265 suggesting that electrostatic and polar interactions may contribute to complex formation (Fig. 3J, S5E, F). Notably, Glu49 of SOD1 was positioned within both the predicted TDP-43 interaction surface and the Amisodin-binding pocket, raising the possibility that Amisodin may influence a local SOD1 surface involved in TDP-43 association (Fig. S9C–E). Although these predictions do not establish direct binding or competition, they provide a testable structural framework for future biochemical studies.

We therefore next asked whether TDP-43-associated pathology was functionally associated with SOD1 in vivo. To address this question, we generated hTDP-43 (+/+);mSOD1 (-/-) double-transgenic mice (Fig. 4A). Genetic ablation of SOD1 substantially mitigated the severe motor dysfunction and neuronal loss observed in hTDP-43-overexpressing mice, providing in vivo evidence that SOD1 contributes significantly to TDP-43-driven neurotoxicity (Fig. 4D-I). However, overall survival was extended by only approximately 5 days (Fig. 4L). The dissociation between marked improvement in motor and neuronal phenotypes and the relatively modest survival benefit suggests that SOD1-dependent mechanisms contribute substantially to TDP-43-associated neurotoxicity but do not account

for all pathological consequences of TDP-43 dysregulation.

The limited survival benefit may partly reflect pathology intrinsic to the hTDP-43 mice, particularly prominent CA3 neuronal loss that was not fully rescued by SOD1 deficiency (Fig. S6F-H). The intrinsic susceptibility of CA3 circuitry to proteostatic stress may therefore contribute to disease severity through mechanisms that are at least partly independent of SOD1 [60-62]. Importantly, this pattern does not fully recapitulate the predominant spinal motor-neuron pathology of human ALS. Thus, although the present model provides strong genetic evidence that SOD1 modulates TDP-43-associated neurotoxicity, it has limitations for defining the interaction specifically within motor neurons. To address this issue, we are developing a motor neuron-specific TDP-43 expression mice to more directly examine the mechanistic relationship between TDP-43 pathology and SOD1 in vivo.

Complete SOD1 ablation is also biologically distinct from selective targeting of pathogenic SOD1 conformers. Because native SOD1 contributes to broader cellular homeostasis [47], constitutive loss of SOD1 removes both toxic SOD1 species and physiological SOD1 functions. This distinction may partly explain why the therapeutic effects of conformer-selective pharmacological intervention are not fully recapitulated by genetic SOD1 deletion. Rather than globally suppressing SOD1, selective targeting of pathogenic conformers may therefore offer a strategy to attenuate SOD1-dependent proteotoxicity while preserving normal SOD1 function.

The genetic findings were further supported by pharmacological intervention. Consistent with the effects of SOD1 depletion, Amisodin markedly reduced cytoplasmic TDP-43 accumulation, preserved neurons, improved motor function, and prolonged survival in hTDP-43 transgenic mice (Fig. 4, 5). Notably, the approximately 10 days extension of survival represents a substantial effect in the context of the highly aggressive hTDP-43 (+/+) phenotype, which otherwise results in death within approximately 21-25 days. The convergence of genetic and pharmacological approaches therefore provides complementary evidence that pathogenic SOD1 intermediates are functionally involved in TDP-43-associated neurotoxicity rather than simply co-occurring with TDP-43 pathology (Fig. 6L).

Several important questions remain. Direct biochemical and structural studies will be required to determine whether trimeric SOD1 physically interacts with TDP-43 at the predicted interface and

whether Amisodin directly disrupts or allosterically modifies this interaction. Motor neuron-specific TDP-43 models and patient-derived cellular systems will also be important for establishing whether the SOD1-TDP-43 axis operates within disease-relevant neuronal populations and across heterogeneous forms of sporadic ALS.

From a translational perspective, an important next step will be to determine whether biomarkers reflecting TDP-43 and SOD1 proteotoxicity can identify patients most likely to benefit from trimer-directed therapy. The clinical development of Tofersen provides an instructive precedent for the importance of biomarker-guided therapeutic development in ALS, as reductions in neurofilament light chain (NfL) emerged as a key pharmacodynamic indicator of biological treatment activity and helped support the assessment of therapeutic benefit. A similar biomarker strategy may be particularly important for extending SOD1-directed approaches beyond genetically defined SOD1-ALS to sporadic ALS, in which patient selection cannot rely on SOD1 genotype alone. In this context, biomarkers that directly capture the SOD1–TDP-43 pathological axis could provide molecular evidence for identifying sporadic ALS patients in whom SOD1 proteotoxicity contributes to downstream TDP-43 dysfunction. Circulating EV-associated TDP-43 correlates with neurofilament levels and clinical severity and is elevated in molecularly confirmed TDP-43 proteinopathy [50], whereas CSF cryptic HDGFL2 provides a complementary readout of impaired nuclear TDP-43 function that can become abnormal before or near clinical disease onset [50]. Together, these putative TDP-43 biomarkers capture distinct aspects of TDP-43 pathology and could therefore support both patient enrichment and pharmacodynamic monitoring in future trials. Furthermore, disease-associated SOD1 conformers could provide an additional layer of molecular stratification by identifying patients with evidence of SOD1 misfolding or proteotoxic stress. Just as NfL played an important role in establishing biological treatment activity during the clinical development of Tofersen, the development and validation of biomarkers that specifically report TDP-43 dysfunction and its relationship to pathological SOD1 may be critical for the clinical development of trimer-directed therapies in sporadic ALS. Such a biomarker-driven approach could ultimately enable SOD1-directed therapy to evolve from a predominantly genotype-defined strategy toward a pathology- and biomarker-defined therapeutic framework encompassing

selected patients with sporadic ALS.

In summary, trimeric SOD1 acts as a convergent pathogenic node linking SOD1 proteotoxicity with TDP-43 mislocalization and aggregation in ALS. Genetic depletion of SOD1 attenuated TDP-43-associated motor dysfunction and neuronal loss, while pharmacological targeting of trimeric SOD1 with Amisodin reduced TDP-43 aggregation, improved functional outcomes and prolonged the lifespan in hTDP-43 transgenic mice. Together, these findings provide genetic and pharmacological evidence that pathogenic SOD1 intermediates contribute to TDP-43-driven neurotoxicity.

Methods

Transgenic mouse

The experiments were performed in the Association for Assessment and Accreditation of Laboratory Animal Care certified facility, in compliance with animal policies approved by by Pusan National University Institutional Animal Care and Use Committee (IACUC). All mice were maintained under 20~23 °C and light-controlled conditions (12/12 h light/dark cycle). hSOD1^{G93A}, hTDP-43, and mSOD1-knockout mouse lines were obtained from The Jackson Laboratory. Homozygous hTDP-43 mice were generated by intercrossing hemizygous hTDP-43 mice, and hTDP-43 (+/+);mSOD1 (-/-) mice were generated by crossing hTDP-43 (+/-);mSOD1 (+/-) breeders. Detailed strain information is provided in Supplementary Methods.

Drug administration and experimental design

The therapeutic efficacy of Amisodin was evaluated in hTDP-43 (+/-), hTDP-43 (+/+) and hSOD1^{G93A} transgenic mouse (Tg) models using multiple independent treatment cohorts. Amisodin was administered orally three times per week at the indicated doses, and control mice received vehicle consisting of 1% HPMC (Hydroxypropyl Methylcellulose) E5, 0.5% PVP (Polyvinylpyrrolidone) K30, and 0.2% SLS (Sodium Lauryl Sulfate) in water.

To evaluate the therapeutic efficacy of Amisodin in hTDP-43 (+/+) offspring, two independent treatment cohorts were established using hTDP-43 (+/-) parental mice. In both cohorts, Amisodin was

orally administered to the parental mice, and its therapeutic effects were subsequently evaluated in the offspring. Amisodin (50 mg/kg) was orally administered to hTDP-43 (+/-) mice three times per week, whereas the control group received vehicle. The two cohorts differed primarily in the duration of Amisodin administration and the period of maternal treatment after mating. In cohort 1, parental mice received Amisodin (50 mg/kg) beginning at 6 months of age and were mated after approximately 1 months of treatment. Treatment was continued in females throughout pregnancy and discontinued after parturition. In cohort 2, treatment was initiated at 3 months of age, mating was performed after approximately 2 months of treatment, and maternal administration was continued throughout pregnancy and lactation until postnatal day 21 (P21). In both cohorts, offspring were euthanized at P21, and brain and spinal cord tissues were collected for histological and/or biochemical analyses.

For direct therapeutic evaluation in hTDP-43 (+/-) mice, treatment was initiated either at 8 months of age with vehicle or Amisodin (20 or 50 mg/kg) for 8 months, or at 10 months of age with vehicle or Amisodin (50 mg/kg) for 6 months. Age-matched wild-type littermates received vehicle. All animals were euthanized at 16 months of age for tissue analysis.

In SOD1 $^{G93A\text{-}Tg}$ mice, vehicle or Amisodin (50 mg/kg) was orally administered three times per week from 9 weeks of age until the defined disease endpoint. Age-matched wild-type littermates receiving vehicle serve as non-transgenic control.

Motor performance assessment

Grip strength test Forelimb and hindlimb grip strength were measured using a grip strength meter (JD-A-22; JEUNGDO BIO&PLANT, Seoul, South Korea). Each mouse was tested 3–5 times, and the mean peak force (N, newtons) was used for analysis.

Vertical grid test The vertical grid test was performed as previously described [30]. Mice were placed near the top of a vertically oriented wire-mesh grid facing upward and allowed to turn and descend voluntarily. Each mouse was tested three times, and the mean value was used for analysis. The time required to turn from the upward- to downward-facing position (time to turn) and the total time required to descend and reach the bottom with the forepaws (total time) were recorded. Detailed apparatus

dimensions and habituation procedures are provided in Supplementary Methods.

Open field test Spontaneous locomotor activity was assessed in a 40 × 40 cm arena for 5 min using Smart 3.0 software.

Rotarod test Motor coordination was assessed using an accelerating rotarod apparatus (B.S. Technolab, Seoul, South Korea). Mice were trained for 2 weeks from 8 weeks of age, and latency to fall was recorded while the rotation speed increased from 5 to 30 rpm over 4 min.

Neurofilament Light Chain (NF-L) analysis

Blood samples were collected from mice by tail tip incision, and approximately 50~100 μL of blood was collected into K_2EDTA-coated microtainer tubes (BD Microtainer, Cat. No. 365974) to prevent coagulation. In $SOD1^{G93A\text{-}Tg}$ mice, blood was collected via tail-tip bleeding at 9, 12, 15, and 17 weeks of age. Plasma samples were collected from homozygous hTDP-43 mice before endpoint and from heterozygous hTDP-43 mice at 16 months of age for NF-L quantification. The samples were centrifuged at 2,000 x g for 10 min at 4 °C, and the resulting plasma was carefully separated and stored at −80 °C until analysis. Plasma samples were diluted 1:250–1:500 prior to analysis. Plasma neurofilament light chain (NF-L) levels were measured using a commercial ELISA kit (UmanDiagnostics, Cat. No. 20-8002) according to the manufacturer's protocol. Absorbance was read at 450 nm using a microplate reader, and NF-L concentrations were determined from a standard curve generated with known concentrations of recombinant NF-L.

Immunohistochemistry

Brain and spinal cord tissues were fixed in 10% formalin for 48 h, paraffin-embedded, and sectioned at 5 μm. Sections from the cervical spinal cord and hippocampus were subjected to hematoxylin and eosin (H&E) staining and immunohistochemistry using antibodies against MAP2, NeuN, and TDP-43. Immunoreactivity was quantified using ImageJ software (version 1.54p). For DAB-based immunohistochemistry, staining intensity was quantified after color deconvolution. Detailed tissue-processing procedures and antibody information are provided in Supplementary Methods.

Bioanalysis of Amisodin

To assess maternal transfer of Amisodin to offspring, WT female mice were treated orally with Amisodin (50 mg/kg, three times per week) before and after mating. Following mating, Amisodin administration was continued in parental female mice during the postnatal period. The total duration of Amisodin administration was approximately 1 month. Offspring were euthanized on postnatal day 18, and plasma, brain, and spinal cord samples were collected for quantitative analysis of Amisodin by liquid liquid chromatography–tandem mass spectrometry (LC-MS/MS). The sample preparation procedures are presented in Supplementary Methods.

Cell lines and reagents

A549, HEK293T and U87MG cells were obtained from the American Type Culture Collection (ATCC), HOG and C20A4 cells from Sigma-Aldrich, and SK-N-SH cells from the Korean Cell Line Bank (KCLB). The human schwannoma cell line Hei-193 cell was kindly provided by Dr. G. Zadeh (University Health Network, Toronto, ON, Canada), and NSC-34 cells were provided by Dr. KH Lee (Pusan National University, Busan, South Korea). All cells were maintained under standard culture conditions. $CoCl_2$ (hypoxia-inducer; C8661) and TPEN (Zn2+ scavenger; P4413) were purchased from Sigma Aldrich (St, Louis, Mo, USA). Detailed culture conditions are provided in Supplementary Methods.

Plasmids, siRNAs and transfection

GFP-Lamin A and GFP-Lamin C expression vectors were provided by T. Misteli and J. Lammerding, respectively. Expression vectors encoding wild-type and mutant SOD1, as well as tdTomato-TDP-43, were obtained from Addgene or generated by site-directed mutagenesis. Plasmids were transfected using jetPEI® or ViaFect™ reagents and siRNAs were introduced using DharmaFECT™ reagent according to the manufacturers' instructions. Detailed plasmid information and siRNA sequences are provided in Supplementary Methods.

Generation of SOD1-knockout HEK293T cells

SOD1-knockout HEK293T cells were generated using CRISPR/Cas9 with an sgRNA targeting exon 2 of human SOD1. Gene editing was performed using the LentiCRISPRv2GFP vector, and knockout clones were validated before use. Detailed sgRNA and oligonucleotide sequences are provided in Supplementary Methods.

Recombinant protein purification

GST-tagged SOD1 (WT, G85R, G93A, and G147P) and TDP-43 recombinant proteins were expressed in *E. coli* BL21(DE3) using the pCold GST (Takara Bio Inc., Kusatsu, Shiga, Japan) vector and purified by glutathione-affinity chromatography (Thermo Fisher Scientific, Waltham, MA, USA).

Protein extraction and western blot analysis

Cell lysates were prepared using RIPA buffer for conventional immunoblotting or mild detergent buffer for native and oligomerization analyses. Glutaraldehyde cross-linking was performed where indicated. Mouse spinal cord tissues were homogenized and fractionated into whole, soluble, and insoluble fractions for immunoblotting and immunoprecipitation. Detailed extraction buffers, fractionation procedures, and antibody information are provided in Supplementary Methods.

Protein–Protein interaction assays

For His pull-down assay, agarose bead-conjugated His-tagged recombinant proteins were incubated with the indicated transfected cell lysates in PBS for 1 hr at room temperature. The beads were then collected, washed with PBS, and the bound proteins were analyzed by SDS-PAGE and immunoblotting.

For in vitro IP assays using recombinant proteins, FLAG-tagged TDP-43 and SOD1 recombinant proteins were incubated together for 15 min at room temperature, followed by precipitation with anti-FLAG agarose beads for an additional 15 min. The beads were washed with RIPA buffer, and bound proteins were analyzed by SDS-PAGE and immunoblotting.

To assess the interaction between misfolded SOD1 and TDP-43 under cellular stress conditions, cell

lysates were subjected to immunoprecipitation with an anti-TDP-43 antibody. Immunoprecipitates were analyzed by SDS-PAGE or Native-PAGE followed by immunoblotting with B8H10 or C4F6 antibodies.

For Amisodin-treated binding assays, SOD1 recombinant protein was pre-incubated with Amisodin for 30 min at room temperature before addition of FLAG-tagged TDP-43. The resulting complexes were subjected to anti-FLAG immunoprecipitation as described above.

Biotin-Amisodin pull down assay

SOD1-knockout HEK293T cells expressing mutant SOD1 were incubated with biotin-conjugated Amisodin. Amisodin-bound proteins were isolated using streptavidin beads and analyzed by SDS-PAGE and immunoblotting. Biotin-Amisodin was chemically synthesized by STA Pharmaceutical (WuXi AppTec, China).

Immunofluorescence staining

Cells grown on coverslips were fixed, permeabilized, blocked, and incubated with the indicated primary and fluorescently labeled secondary antibodies. Nuclei were counterstained with DAPI, and fluorescence images were acquired using LSM 900 microscope (NFEC-2025-01-302966) equipped with Airyscan 2, ApoTome2 imaging system, CELENA X imaging system.

Cells containing SOD1 or TDP-43 aggregates were quantified in randomly selected fields and expressed as a percentage of the total number of cells analyzed. Cell counting was independently performed by three observers blinded to the transfection and treatment conditions.

For tissue immunofluorescence, sections were stained with antibodies against MAP2, NeuN, and TDP-43, and fluorescence intensity was quantified using ImageJ software (version 1.54p). Detailed staining and imaging procedures are provided in Supplementary Methods.

Molecular docking

Protein–protein docking between SOD1 and TDP-43 was performed using the ClusPro web server. TDP-43 RRM1–RRM2 (PDB ID: 4BS2), TDP-43 N-terminal domain (PDB ID: 2N4P), and human

SOD1 monomer/dimer structures (PDB ID: 1HL5) were used together with a previously reported non-native SOD1 trimer model [31]. Predicted binding affinities of the SOD1–TDP-43 complexes were estimated using the PRODIGY web server, and docked complexes were visualized using UCSF ChimeraX.

Docking of Amisodin to the SOD1 trimer was performed using AutoDock Vina v1.2.7. Blind docking was followed by focused docking at the top-ranked binding region, and the lowest-energy binding pose was analyzed using BIOVIA Discovery Studio Visualizer 2025. Detailed structure preparation and docking procedures are provided in Supplementary Methods.

Statistical analysis

Statistical analysis was done by GraphPad Prism 10.0. Data were analyzed using unpaired Student's *t*-tests for comparisons between two groups. Values with $P < 0.05$ were considered statistically significant. Error bars represent the standard deviation (SD). All data are presented as mean ± SD from at least three independent experiments.

Abbreviations

ALS	Amyotrophic lateral sclerosis
TDP-43	TAR DNA-binding protein 43
SOD1	Superoxide dismutase 1
LMB	Leptomycin B
RRM	RNA recognition motif
N	Newtons
IP	Immunoprecipitation
NF-L	Neurofilament light chain
Tg	Transgenic
PAMPA	Parallel Artificial Membrane Permeability Assay
BBB	Blood-Brain Barrier

PDB Protein Data Bank

References

1. Statland, J. M., Barohn, R. J., McVey, A. L., Katz, J. & Dimachkie, M. M. Patterns of weakness, classification of motor neuron disease & clinical diagnosis of sporadic ALS. *Neurol. Clin.* **33**, 735 (2015).

2. Longinetti, E. & Fang, F. Epidemiology of amyotrophic lateral sclerosis: an update of recent literature. *Curr. Opin. Neurol.* **32**, 771–776 (2019).

3. Brown, C. A., Lally, C., Kupelian, V. & Flanders, W. D. Estimated prevalence and incidence of amyotrophic lateral sclerosis and SOD1 and C9orf72 genetic variants. *Neuroepidemiology* **55**, 342–353 (2021).

4. Brown, R. H. & Al-Chalabi, A. Amyotrophic lateral sclerosis. *N. Engl. J. Med.* **377**, 162–172 (2017).

5. Mead, R. J., Shan, N., Reiser, H. J., Marshall, F. & Shaw, P. J. Amyotrophic lateral sclerosis: a neurodegenerative disorder poised for successful therapeutic translation. *Nature Reviews Drug Discovery* **22**, 185–212 (2023).

6. Xu, X. *et al*. A perspective on therapies for amyotrophic lateral sclerosis: can disease progression be curbed? *Translational neurodegeneration* **10**, 29 (2021).

7. Petrov, D., Mansfield, C., Moussy, A. & Hermine, O. ALS clinical trials review: 20 years of failure. Are we any closer to registering a new treatment? *Frontiers in aging neuroscience* **9**, 68 (2017).

8. Chiò, A., Calvo, A., Moglia, C., Mazzini, L. & Mora, G. Phenotypic heterogeneity of amyotrophic lateral sclerosis: a population based study. *Journal of Neurology, Neurosurgery & Psychiatry* **82**, 740–746 (2011).

9. Taylor, J. P., Brown Jr, R. H. & Cleveland, D. W. Decoding ALS: from genes to mechanism. *Nature* **539**, 197–206 (2016).

10. Neupane, K. *et al*. Direct observation of prion-like propagation of protein misfolding templated by pathogenic mutants. *Nature Chemical Biology* **20**, 1220–1226 (2024).

11. Suk, T. R. & Rousseaux, M. W. The role of TDP-43 mislocalization in amyotrophic lateral sclerosis. *Molecular neurodegeneration* **15**, 45 (2020).

12. Hergesheimer, R. C. *et al*. The debated toxic role of aggregated TDP-43 in amyotrophic lateral sclerosis: a resolution in sight? *Brain* **142**, 1176–1194 (2019).

13. Kabashi, E., Valdmanis, P. N., Dion, P. & Rouleau, G. A. Oxidized/misfolded superoxide dismutase-1: the cause of all amyotrophic lateral sclerosis? *Annals of Neurology: Official Journal of the American Neurological Association and the Child Neurology Society* **62**, 553–559 (2007).

14. Rosen, D. R. *et al*. Mutations in Cu/Zn superoxide dismutase gene are associated with familial amyotrophic lateral sclerosis. *Nature* **362**, 59–62 (1993).

15. De Boer, E. M. J. *et al*. TDP-43 proteinopathies: a new wave of neurodegenerative diseases. *Journal of Neurology, Neurosurgery & Psychiatry* **92**, 86–95 (2021).

16. Scotter, E. L., Chen, H. & Shaw, C. E. TDP-43 proteinopathy and ALS: insights into disease mechanisms and therapeutic targets. *Neurotherapeutics* **12**, 352–363 (2015).

17. Lee, E. B., Lee, V. M. & Trojanowski, J. Q. Gains or losses: molecular mechanisms of TDP43-mediated neurodegeneration. *Nature Reviews Neuroscience* **13**, 38–50 (2012).

18. Trist, B. G. *et al*. Co-deposition of SOD1, TDP-43 and p62 proteinopathies in ALS: evidence for multifaceted pathways underlying neurodegeneration. *Acta Neuropathologica Communications* **10**, 122 (2022).

19. Pokrishevsky, E. *et al*. Aberrant localization of FUS and TDP43 is associated with misfolding of SOD1 in amyotrophic lateral sclerosis. *PloS one* **7**, e35050 (2012).

20. Pokrishevsky, E., Grad, L. I. & Cashman, N. R. TDP-43 or FUS-induced misfolded human wild-type SOD1 can propagate intercellularly in a prion-like fashion. *Scientific reports* **6**, 22155 (2016).

21. Zeineddine, R., Farrawell, N. E., Lambert-Smith, I. A. & Yerbury, J. J. Addition of exogenous SOD1 aggregates causes TDP-43 mislocalisation and aggregation. *Cell Stress and Chaperones* **22**, 893–902 (2017).

22. Pokrishevsky, E. *et al*. Tryptophan residues in TDP-43 and SOD1 modulate the cross-seeding and toxicity of SOD1. *J. Biol. Chem.* **300**, 107207 (2024).

23. Tsekrekou, M., Giannakou, M., Papanikolopoulou, K. & Skretas, G. Protein aggregation and therapeutic strategies in SOD1-and TDP-43-linked ALS. *Frontiers in Molecular Biosciences* **11**, 1383453 (2024).

24. Wilson, D. M. *et al*. Hallmarks of neurodegenerative diseases. *Cell* **186**, 693–714 (2023).

25. Scheckel, C. & Aguzzi, A. Prions, prionoids and protein misfolding disorders. *Nature Reviews Genetics* **19**, 405–418 (2018).

26. Prusiner, S. B. Neurodegenerative diseases and prions. *N. Engl. J. Med.* **344**, 1516–1526 (2001).

27. McAlary, L. *et al*. Amyotrophic lateral sclerosis: proteins, proteostasis, prions, and promises. *Frontiers in Cellular Neuroscience* **14**, 581907 (2020).

28. Woo, T. *et al*. Novel chemical inhibitor against SOD1 misfolding and aggregation protects neuron-loss and ameliorates disease symptoms in ALS mouse model. *Communications biology* **4**, 1397 (2021).

29. Woo, T. *et al*. Inhibition of SOD1 trimerization is a novel drug target for ALS disease. *Translational Neurodegeneration* **14**, 21 (2025).

30. Kim, S. T., Son, H. J., Choi, J. H., Ji, I. J. & Hwang, O. Vertical grid test and modified horizontal grid test are sensitive methods for evaluating motor dysfunctions in the MPTP mouse model of Parkinson's disease. *Brain Res.* **1306**, 176–183 (2010).

31. Choi, E. S., Hnath, B., Sha, C. M. & Dokholyan, N. V. Unveiling the double-edged sword: SOD1 trimers possess tissue-selective toxicity and bind septin-7 in motor neuron-like cells. *Structure* **32**, 1776–1792. e5 (2024).

32. Mackenzie, I. R. *et al*. Pathological TDP-43 distinguishes sporadic amyotrophic lateral sclerosis from amyotrophic lateral sclerosis with SOD1 mutations. *Annals of Neurology: Official Journal of the American Neurological Association and the Child Neurology Society* **61**, 427–434 (2007).

33. Proctor, E. A. *et al*. Nonnative SOD1 trimer is toxic to motor neurons in a model of amyotrophic lateral sclerosis. *Proceedings of the National Academy of Sciences* **113**, 614–619 (2016).

34. Yang, C. *et al*. Low-level overexpression of wild type TDP-43 causes late-onset, progressive neurodegeneration and paralysis in mice. *PLoS One* **17**, e0255710 (2022).

35. Wils, H. *et al*. TDP-43 transgenic mice develop spastic paralysis and neuronal inclusions characteristic of ALS and frontotemporal lobar degeneration. *Proceedings of the National Academy of Sciences* **107**, 3858–3863 (2010).

36. Hampoelz, B. & Baumbach, J. Nuclear envelope assembly and dynamics during development. **133**, 96–106 (2023).

37. Vergnes, L., Péterfy, M., Bergo, M. O., Young, S. G. & Reue, K. Lamin B1 is required for mouse development and nuclear integrity. *Proceedings of the National Academy of Sciences* **101**, 10428–10433 (2004).

38. Lopez-Soler, R. I., Moir, R. D., Spann, T. P., Stick, R. & Goldman, R. D. A role for nuclear lamins in nuclear envelope assembly. *J. Cell Biol.* **154**, 61 (2001).

39. Rodemer, W. *et al*. Network Dysfunction Precedes Neurodegeneration in a dox-Regulatable TDP-43 Mouse Model of ALS-FTD. *Journal of Neuroscience* **45** (2025).

40. LaClair, K. D. *et al*. Depletion of TDP-43 decreases fibril and plaque β-amyloid and exacerbates neurodegeneration in an Alzheimer's mouse model. *Acta Neuropathol.* **132**, 859–873 (2016).

41. Basso, M. *et al*. Insoluble mutant SOD1 is partly oligoubiquitinated in amyotrophic lateral sclerosis mice. *J. Biol. Chem.* **281**, 33325–33335 (2006).

42. Gill, C. *et al*. SOD1-positive aggregate accumulation in the CNS predicts slower disease progression and increased longevity in a mutant SOD1 mouse model of ALS. *Scientific reports* **9**, 6724 (2019).

43. Feldman, E. L. *et al*. Amyotrophic lateral sclerosis. *The Lancet* **400**, 1363–1380 (2022).

44. Witzel, S. *et al*. Population-Based Evidence for the Use of Serum Neurofilaments as Individual Diagnostic and Prognostic Biomarkers in Amyotrophic Lateral Sclerosis. *Ann. Neurol.* **96**, 1040–1057 (2024).

45. Meyer, T. *et al*. Clinical and patient-reported outcomes and neurofilament response during tofersen treatment in SOD1-related ALS—A multicenter observational study over 18 months. *Muscle Nerve* **70**, 333–345 (2024).

46. Miller, T. M. *et al*. Trial of antisense oligonucleotide tofersen for SOD1 ALS. *N. Engl. J. Med.* **387**, 1099–1110 (2022).

47. Zheng, Y. *et al*. SOD1 is delivered to lysosomes via autophagy to maintain lysosomal function and integrity. *J. Cell Biol.* **224**, e202501007 (2025).

48. Maier, M. *et al*. A human-derived antibody targets misfolded SOD1 and ameliorates motor symptoms in mouse models of amyotrophic lateral sclerosis. *Science translational medicine* **10**, eaah3924 (2018).

49. Guan, T. *et al*. Selective removal of misfolded SOD1 delays disease onset in a mouse model of amyotrophic lateral sclerosis. *Cellular and Molecular Life Sciences* **80**, 304 (2023).

50. Dong, Q., Zhu, J., Liu, S., Yu, X. & Liu, R. An oligomer-specific antibody improved motor function and attenuated neuropathology in the SOD1-G93A transgenic mouse model of ALS. *Int. Immunopharmacol.* **65**, 413–421 (2018).

51. Proceedings of the 24th Annual NEALS Meeting*Muscle & Nerve* **72**, S1–S97 (2025).

52. Pongrácová, E., Buratti, E. & Romano, M. Prion-like spreading of disease in TDP-43 proteinopathies. *Brain Sciences* **14**, 1132 (2024).

53. Gosset, P., Camu, W., Raoul, C. & Mezghrani, A. Prionoids in amyotrophic lateral sclerosis. *Brain Communications* **4**, fcac145 (2022).

54. Jo, M. *et al*. The role of TDP-43 propagation in neurodegenerative diseases: integrating insights from clinical and experimental studies. *Exp. Mol. Med.* **52**, 1652–1662 (2020).

55. Irwin, K. E. *et al*. A fluid biomarker reveals loss of TDP-43 splicing repression in presymptomatic ALS–FTD. *Nat. Med.* **30**, 382–393 (2024).

56. Theunissen, F. *et al*. Entering the era of precision medicine to treat amyotrophic lateral sclerosis. *Molecular neurodegeneration* **20**, 111 (2025).

57. Van Daele, S. H., Masrori, P., Van Damme, P. & Van Den Bosch, L. The sense of antisense therapies in ALS. *Trends Mol. Med.* **30**, 252–262 (2024).

58. Choi, E. S. & Dokholyan, N. V. SOD1 oligomers in amyotrophic lateral sclerosis. *Curr. Opin. Struct. Biol.* **66**, 225–230 (2021).

59. Das, B. *et al*. A Zn-dependent structural transition of SOD1 modulates its ability to undergo phase separation. *EMBO J.* **42**, e111185 (2023).

60. Oh, M. M., Simkin, D. & Disterhoft, J. F. Intrinsic hippocampal excitability changes of opposite signs and different origins in CA1 and CA3 pyramidal neurons underlie aging-related cognitive deficits. *Frontiers in systems neuroscience* **10**, 52 (2016).

61. Mohar, B. *et al*. DELTA: a method for brain-wide measurement of synaptic protein turnover reveals localized plasticity during learning. *Nat. Neurosci.*, 1–10 (2025).

62. Jamshidi, P. *et al*. Distribution of TDP-43 pathology in hippocampal synaptic relays suggests transsynaptic propagation in frontotemporal lobar degeneration. *Journal of Neuropathology & Experimental Neurology* **79**, 585–591 (2020).

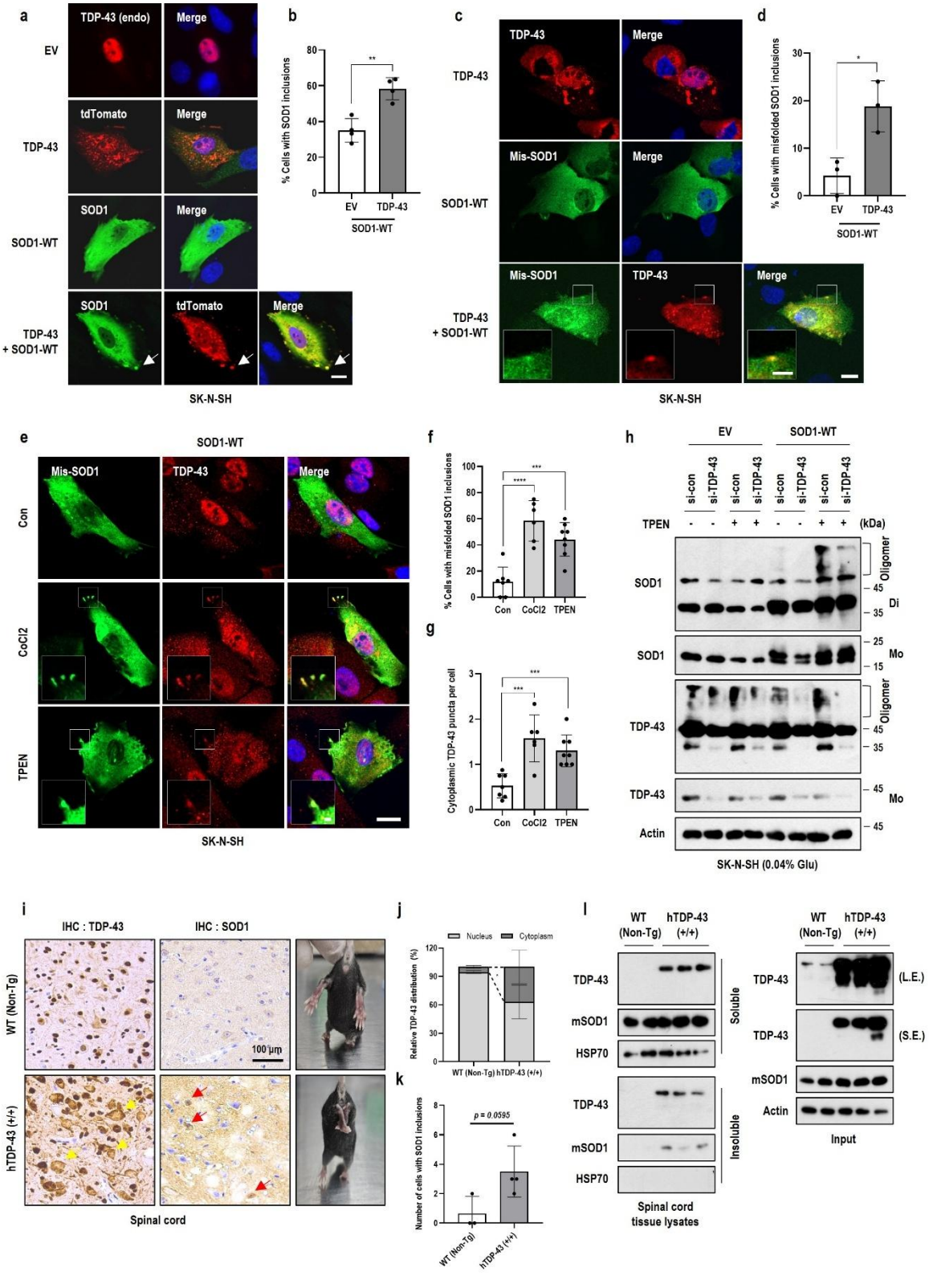

a
TDP-43 (endo)
Merge
EV
tdTomato
TDP-43
SOD1
SOD1-WT
TDP-43
+ SOD1-WT
SK-N-SH
b
% Cells with SOD1 inclusions
EV
TDP-43
SOD1-WT
c
Mis-SOD1
d
% Cells with misfolded SOD1 inclusions
e
Con
CoCl2
TPEN
f
% Cells with misfolded SOD1 inclusions
g
Cytoplasmic TDP-43 puncta per cell
h
EV
SOD1-WT
si-con
si-TDP-43
TPEN
(kDa)
Oligomer
Di
Mo
Actin
SK-N-SH (0.04% Glu)
i
IHC : TDP-43
IHC : SOD1
WT (Non-Tg)
hTDP-43 (+/+)
100 μm
Spinal cord
j
Nucleus
Cytoplasm
Relative TDP-43 distribution (%)
k
p = 0.0595
Number of cells with SOD1 inclusions
l
WT (Non-Tg)
hTDP-43 (+/+)
TDP-43
mSOD1
HSP70
Soluble
Insoluble
(L.E.)
(S.E.)
Actin
Input
Spinal cord tissue lysates

Fig. 1 Mislocalized cytoplasmic TDP-43 promotes aberrant aggregation of WT-SOD1. **a, b** TDP-43 promoted the formation of WT-SOD1 inclusions in SK-N-SH cells. Scale bar, 10 μm. Inclusion-positive cells (white arrows) were counted, and the percentages are presented as mean ± SD (**b**). $^{**}p < 0.01$. **c, d** TDP-43 promoted the formation of misfolded SOD1 inclusions. Misfolded SOD1 detected by B8H10. Scale bar, 10 μm; enlarged images, 5 μm. $^{*}p < 0.05$. **e-g** Upon exposure to cellular stress, misfolded SOD1 inclusions colocalized with cytoplasmic TDP-43 puncta. Scale bar, 10 μm; enlarged images, 2 μm. Misfolded SOD1 inclusion-positive cells (**f**) and cytoplasmic TDP-43 puncta per cell (**g**) were counted, and the percentages are presented as mean ± SD. $^{***}p < 0.001$, $^{****}p < 0.0001$. **h** WT-SOD1 exposed to TPEN formed SOD1 oligomers, which were reduced by TDP-43 knockdown. Glu indicated glutaraldehyde fixation. Di (Dimer), Mo (Monomer). **I-k** Cytoplasmic TDP-43 mislocalization and mSOD1 inclusions were observed in spinal motor neurons of hTDP-43 (+/+) mice. Scale bar, 100 μm. Compared with WT (Non-Tg) mice, hTDP-43 (+/+) mice showed an impaired hindlimb clasping response. The relative nuclear and cytoplasmic distribution of TDP-43 was quantified by cell counting (yellow arrows), and the percentages are presented as mean ± SD (**j**). WT (n=3), hTDP-43 (+/+) (n=5). $^{*}p < 0.05$. SOD1 inclusion-positive cells (red arrows) were counted (**k**). **l** Compared with WT mice, TDP-43 and mSOD1 accumulation was increased in the insoluble fraction of spinal cord lysates from hTDP-43 (+/+) mice.

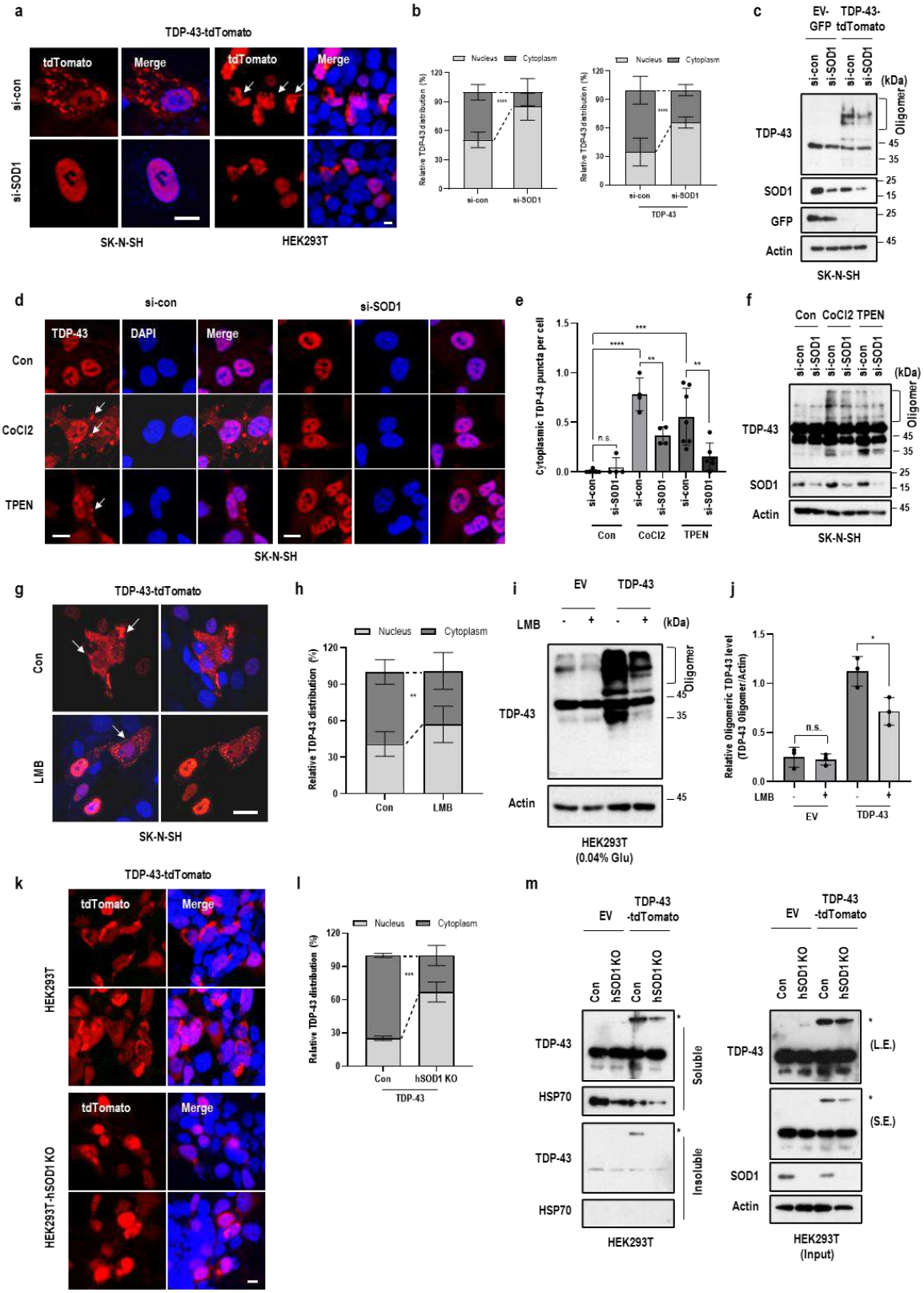

a
TDP-43-tdTomato
si-con
si-SOD1
tdTomato
Merge
SK-N-SH
HEK293T
b
Nucleus
Cytoplasm
Relative TDP-43 distribution (%)
si-con
si-SOD1
TDP-43
c
EV-GFP
TDP-43-tdTomato
(kDa)
Oligomer
TDP-43
SOD1
GFP
Actin
SK-N-SH
d
si-con
si-SOD1
Con
CoCl2
TPEN
TDP-43
DAPI
Merge
SK-N-SH
e
Cytoplasmic TDP-43 puncta per cell
n.s.
Con
CoCl2
TPEN
f
Con
CoCl2
TPEN
SK-N-SH
g
TDP-43-tdTomato
Con
LMB
SK-N-SH
h
Relative TDP-43 distribution (%)
i
EV
TDP-43
LMB
HEK293T
(0.04% Glu)
j
Relative Oligomeric TDP-43 level
(TDP-43 Oligomer/Actin)
k
TDP-43-tdTomato
HEK293T
HEK293T-hSOD1 KO
l
hSOD1 KO
m
EV
TDP-43 -tdTomato
Con
hSOD1 KO
Soluble
Insoluble
HSP70
(L.E.)
(S.E.)
HEK293T
HEK293T
(Input)

Fig. 2 SOD1 depletion attenuates TDP-43 aggregation and cytoplasmic mislocalization. **a, b** SOD1 knockdown reduced cytoplasmic TDP-43 mislocalization and aggregation in SK-N-SH and HEK293T cells. Scale bar, 10 μm. The relative nuclear and cytoplasmic distribution of TDP-43 was quantified by cell counting, and the percentages are presented as mean ± SD (**b**). TDP-43 overexpressing cells transfected with si-RNA were analyzed. [SK-N-SH; si-con (n=9), si-SOD1 (n=8), HEK293T; si-con (n=8), si-SOD1 (n=8)]. ****$p < 0.0001$. **c** TDP-43 oligomerization induced by TDP-43 overexpression was reduced by SOD1 knockdown. **d, e** SOD1 knockdown attenuated the formation of cytoplasmic TDP-43 puncta induced by cellular stress. Scale bar, 10 μm. Cytoplasmic TDP-43 puncta per cell were counted, and the percentages are presented as mean ± SD (**e**). **$p < 0.01$, ***$p < 0.001$, ****$p < 0.0001$. **f** Cellular stress-induced TDP-43 oligomerization was attenuated by SOD1 knockdown. **g, h** LMB (10 μM) treatment attenuated the cytoplasmic TDP-43 mislocalization. Scale bar, 10 μm. The relative nuclear and cytoplasmic distribution of TDP-43 was quantified by cell counting, and the percentages are presented as mean ± SD (**h**). Con (n=15), LMB (n=15). **$p < 0.01$. **i, j** LMB reduced TDP-43 overexpression-induced oligomerization (**i**). Quantification of TDP-43 oligomerization (**j**). *$p < 0.05$. **k, l** Cytoplasmic TDP-43 mislocalization induced by TDP-43 overexpression was attenuated in HEK293T hSOD1 KO cells (**k**). Scale bar, 10 mm. The relative nuclear and cytoplasmic distribution of TDP-43 was quantified by cell counting, and the percentages are presented as mean ± SD (**l**). Control (n=3) and SOD1 KO (n=4) cells overexpressing TDP-43 were analyzed. ***$p < 0.001$. **m** Insoluble TDP-43 accumulation induced by TDP-43 overexpression was reduced in hSOD1 KO cells compared with control cells.

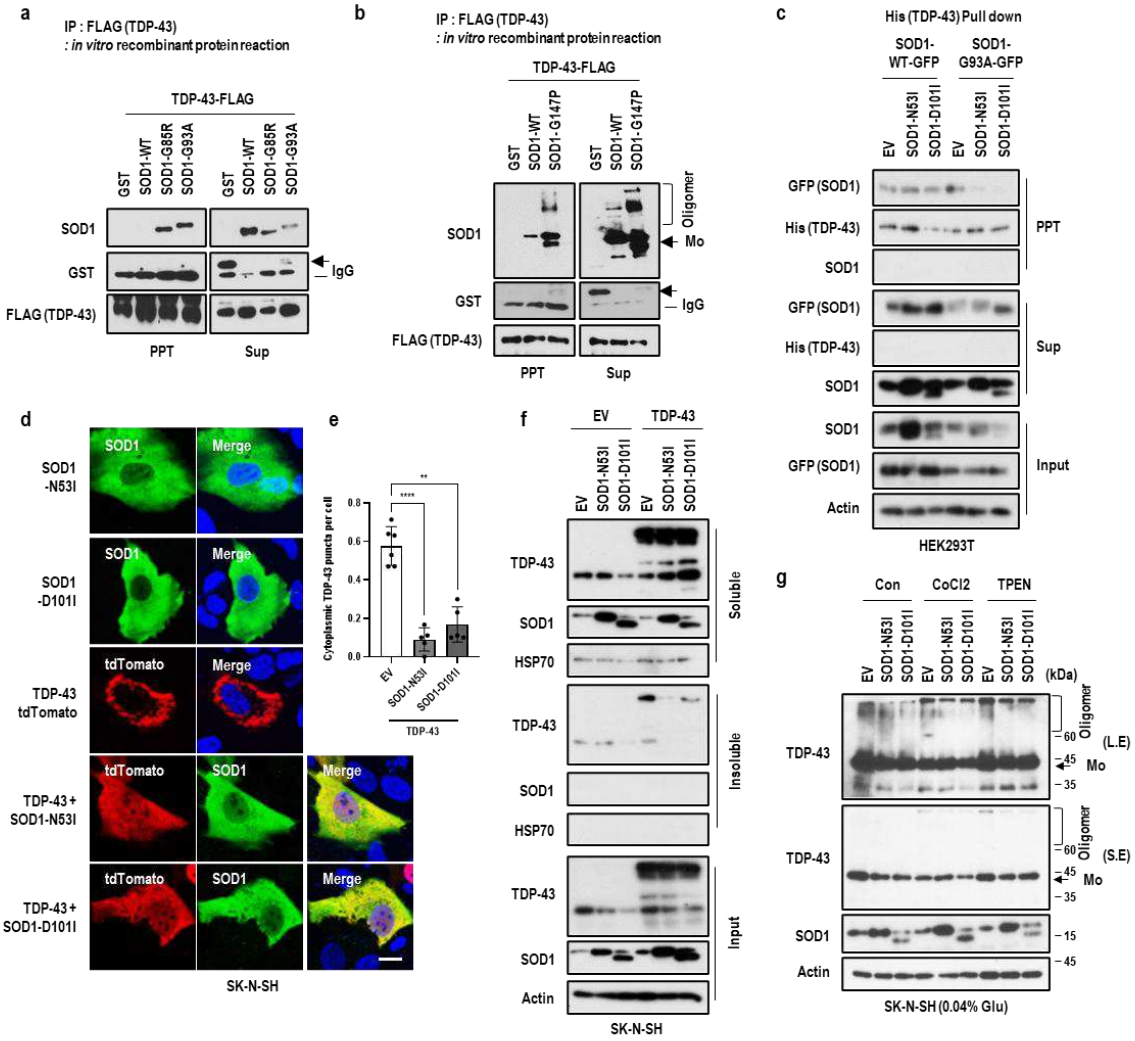

a
IP : FLAG (TDP-43)
: in vitro recombinant protein reaction
TDP-43-FLAG
GST
SOD1-WT
SOD1-G85R
SOD1-G93A
SOD1
GST
IgG
FLAG (TDP-43)
PPT
Sup
b
IP : FLAG (TDP-43)
: in vitro recombinant protein reaction
TDP-43-FLAG
GST
SOD1-WT
SOD1-G147P
Oligomer
Mo
SOD1
GST
IgG
FLAG (TDP-43)
PPT
Sup
c
His (TDP-43) Pull down
SOD1-WT-GFP
SOD1-G93A-GFP
EV
SOD1-N53I
SOD1-D101I
GFP (SOD1)
His (TDP-43)
SOD1
PPT
Sup
Input
Actin
HEK293T
d
SOD1 -N53I
SOD1 -D101I
TDP-43 tdTomato
TDP-43 + SOD1-N53I
TDP-43 + SOD1-D101I
tdTomato
SOD1
Merge
SK-N-SH
e
Cytoplasmic TDP-43 puncts per cell
EV
SOD1-N53I
SOD1-D101I
TDP-43
f
EV
TDP-43
SOD1-N53I
SOD1-D101I
TDP-43
SOD1
HSP70
Soluble
Insoluble
Input
Actin
SK-N-SH
g
Con
CoCl2
TPEN
(kDa)
Oligomer
Mo
(L.E)
(S.E)
SK-N-SH (0.04% Glu)
h
His (SOD1-WT) pull down with HEK293T (TDP-43 domain O/E) lysates
EV-GFP
TDP WT-HA
TDP 1-101-HA
TDP 102-269-HA
TDP 1-266-Flag
TDP 274-343-GFP
TDP 344-414-GFP
TDP Δ102-269-HA
HA
Flag
GFP
His
PPT
Sup
Input
i
N-terminal domain (NTD)
RNA Recognition Motif (RRM)
C-terminal domain (Low-Complexity domain)
j
SOD1 trimer
TDP-43 RRM1-2

Fig. 3 Interaction of TDP-43 with trimer-associated SOD1 promotes reciprocal protein aggregation. **a, b** Recombinant mutant SOD1 (G85R, G93A) (**a**) and the trimer-stabilizing SOD1 mutant (G147P) (**b**) exhibited stronger binding to TDP-43 compared with WT-SOD1. Co-IP assay using FLAG antibody against recombinant proteins (SOD1-WT, G85R, G93A, G147P) and TDP-43-FLAG proteins. Mo (Monomer). **c** SOD1 trimer-destabilizing mutants (N53I, D101I) reduced the interaction between TDP-43 and SOD1-G93A. Cell lysates expressing SOD1-WT, G93A or SOD1-N53I, D101I were incubated with His-TDP-43 protein. **d, e** SOD1 trimer-destabilizing mutants (N53I, D101I) markedly reduced cytoplasmic TDP-43 puncta. Scale bar, 10 μm. The relative nuclear and cytoplasmic distribution of TDP-43 was quantified by cell counting, and the percentages are presented as mean ± SD (**e**). $^{**}p < 0.01$, $^{****}p < 0.0001$. **f** TDP-43 overexpression-induced insoluble TDP-43 was reduced by SOD1 trimer-destabilizing mutant. **g** Cellular stress-induced TDP-43 oligomerization was reduced by SOD1 trimer-destabilizing mutants. Mo (Monomer), L.E (Long Exposure), S.E (Short Exposure). **h** WT-SOD1 interacted with TDP-43 102-269 domain. His tagged SOD1-WT pull down assay was performed using HEK293T lysates expressing the TDP-43 domain. **i** Map of TDP-43 domain. **j** *In silico* prediction of the SOD1 trimer and TDP-43 RRM1-2 interaction interface. Predicted docking model of the SOD1 trimer-TDP-43 RRM1-2 complex and representative interacting residues are shown.

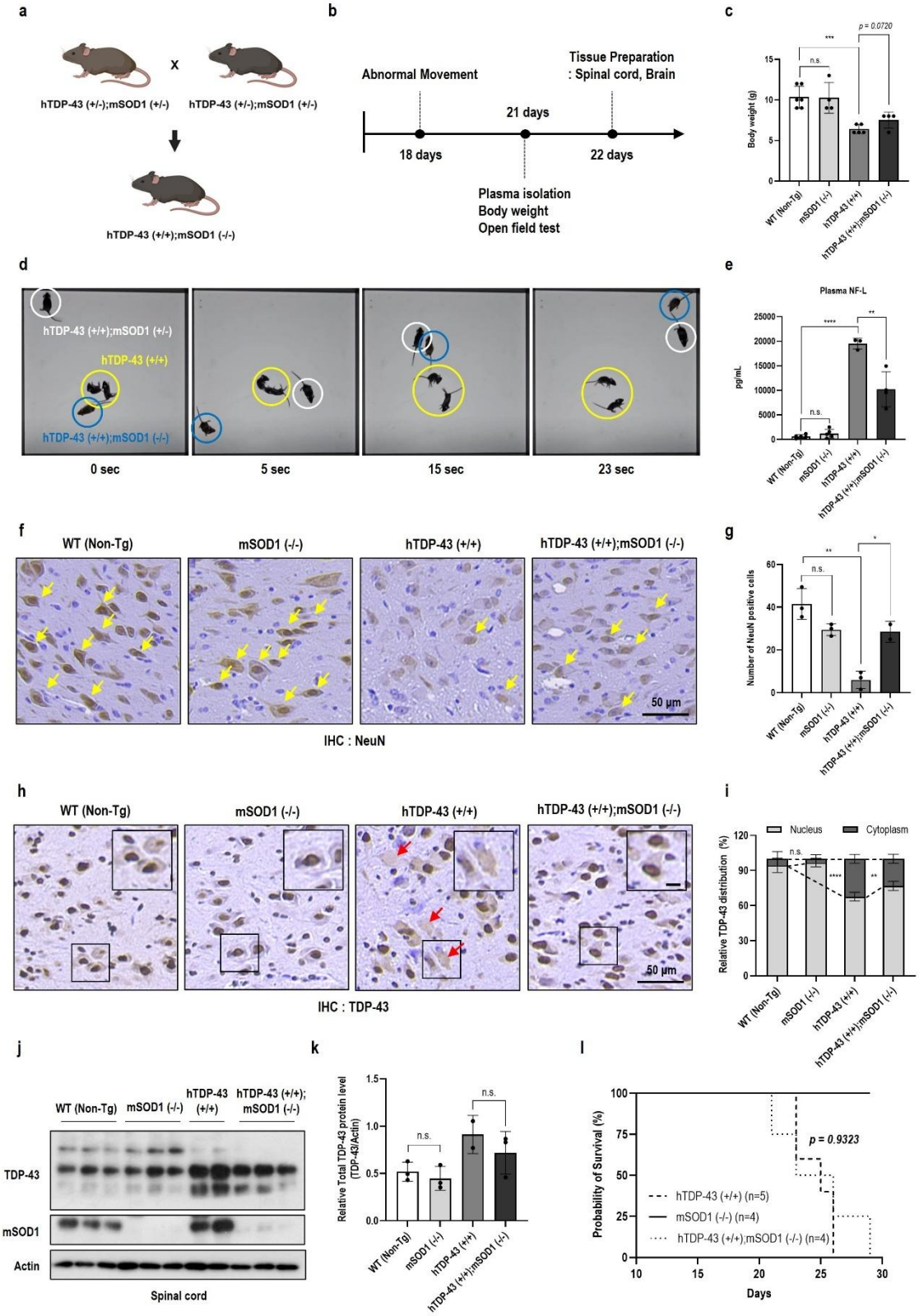

a
hTDP-43 (+/-);mSOD1 (+/-)
x
hTDP-43 (+/-);mSOD1 (+/-)
hTDP-43 (+/+);mSOD1 (-/-)
b
Abnormal Movement
Tissue Preparation
: Spinal cord, Brain
21 days
18 days
22 days
Plasma isolation
Body weight
Open field test
c
Body weight (g)
p = 0.0720
***
n.s.
WT (Non-Tg)
mSOD1 (-/-)
hTDP-43 (+/+)
hTDP-43 (+/+);mSOD1 (-/-)
d
hTDP-43 (+/+);mSOD1 (+/-)
hTDP-43 (+/+)
hTDP-43 (+/+);mSOD1 (-/-)
0 sec
5 sec
15 sec
23 sec
e
Plasma NF-L
pg/mL
****
**
n.s.
f
WT (Non-Tg)
mSOD1 (-/-)
hTDP-43 (+/+)
hTDP-43 (+/+);mSOD1 (-/-)
50 μm
IHC : NeuN
g
Number of NeuN positive cells
**
*
n.s.
h
WT (Non-Tg)
mSOD1 (-/-)
hTDP-43 (+/+)
hTDP-43 (+/+);mSOD1 (-/-)
50 μm
IHC : TDP-43
i
Nucleus
Cytoplasm
Relative TDP-43 distribution (%)
n.s.
****
**
j
WT (Non-Tg)
mSOD1 (-/-)
hTDP-43 (+/+)
hTDP-43 (+/+); mSOD1 (-/-)
TDP-43
mSOD1
Actin
Spinal cord
k
Relative Total TDP-43 protein level (TDP-43/Actin)
n.s.
n.s.
l
Probability of Survival (%)
p = 0.9323
hTDP-43 (+/+) (n=5)
mSOD1 (-/-) (n=4)
hTDP-43 (+/+);mSOD1 (-/-) (n=4)
Days

Fig. 4 SOD1 knockout attenuates TDP-43-associated pathology in hTDP-43 Tg mice. **a** hTDP-43 (+/-);mSOD1 (+/-) mice were crossed to generate hTDP-43 (+/+);mSOD1 (-/-) offspring lacking the mSOD1 background. **b** Experimental design to evaluate motor function and therapeutic effects in the neurodegenerative disease model. **c** hTDP-43 (+/+) mice (n=5) exhibited a significant reduction in body weight relative to WT (Non-Tg) mice (n=6). The loss of body weight was not recovered in hTDP-43 (+/-);mSOD1 (+/-) mice (n=4). **d** hTDP-43 (+/+);mSOD1 (-/-) mice exhibited improved locomotor activity compared with hTDP-43 (+/+) mice. Representative movement traces captured at 5 sec intervals were shown. Recorded behaviors in the open-field test are presented in Additional file 1. **e** Blood plasma NF-L levels were reduced in hTDP-43 (+/+);mSOD1 (-/-) mice (n=4) compared with hTDP-43 (+/+) mice (n=3). **f, g** Reduced NeuN levels in hTDP-43 (+/+) mice (n=3) were restored in hTDP-43 (+/+);mSOD1 (-/-) mice (n=2). Immunohistochemical analysis of NeuN in cervical spinal cord sections from mice (**f**). Scale bar, 50 μm. The number of NeuN-positive cells (yellow arrows) was counted (**g**). *$p < 0.05$, **$p < 0.01$. **h, i** Compared with WT mice (n=6), hTDP-43 (+/+) mice (n=6) exhibited increased cytoplasmic TDP-43 mislocalization (red arrows), which was reduced in hTDP-43 (+/+);mSOD1 (-/-) mice (n=5). mSOD1 (-/-) mice (n=6). Scale bar, 50 μm; enlarged image, 10 μm. The relative nuclear and cytoplasmic distribution of TDP-43 was quantified by cell counting, and the percentages are presented as mean ± SD (**i**). **$p < 0.01$, ****$p < 0.0001$. **j, k** Total TDP-43 expression was unchanged by mSOD1 knockout. Spinal cord lysates were analyzed by western blotting (**j**), and TDP-43 protein levels were quantified (**k**). **l** Compared to hTDP-43 (+/+) mice (n=5), hTDP-43 (+/+);mSOD1 (-/-) mice (n=4) show a modest extension of lifespan.

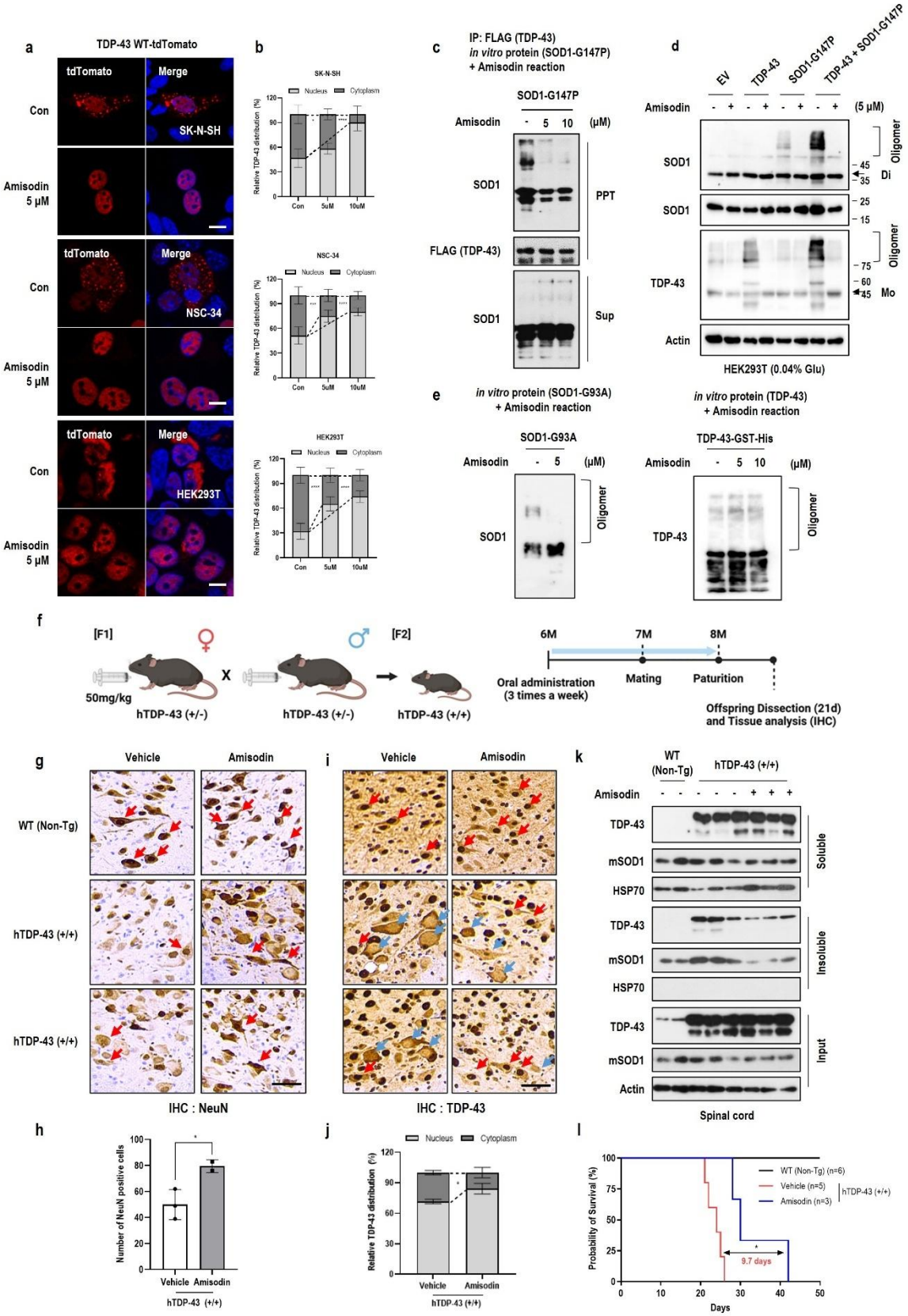

a
TDP-43 WT-tdTomato
tdTomato
Merge
Con
SK-N-SH
Amisodin 5 μM
NSC-34
HEK293T
b
SK-N-SH
NSC-34
HEK293T
Nucleus
Cytoplasm
Relative TDP-43 distribution (%)
Con
5uM
10uM
c
IP: FLAG (TDP-43)
in vitro protein (SOD1-G147P)
+ Amisodin reaction
SOD1-G147P
Amisodin - 5 10 (μM)
SOD1
PPT
FLAG (TDP-43)
Sup
d
EV
TDP-43
SOD1-G147P
TDP-43 + SOD1-G147P
Amisodin - + - + - + - + (5 μM)
SOD1
Oligomer
Di
TDP-43
Mo
Actin
HEK293T (0.04% Glu)
e
in vitro protein (SOD1-G93A)
+ Amisodin reaction
SOD1-G93A
Amisodin - 5 (μM)
in vitro protein (TDP-43)
+ Amisodin reaction
TDP-43-GST-His
Amisodin - 5 10 (μM)
f
[F1]
[F2]
50mg/kg
hTDP-43 (+/-)
hTDP-43 (+/-)
hTDP-43 (+/+)
6M
7M
8M
Oral administration
(3 times a week)
Mating
Paturition
Offspring Dissection (21d)
and Tissue analysis (IHC)
g
Vehicle
Amisodin
WT (Non-Tg)
hTDP-43 (+/+)
hTDP-43 (+/+)
IHC : NeuN
i
IHC : TDP-43
k
WT (Non-Tg)
hTDP-43 (+/+)
Amisodin - - - - + + +
TDP-43
mSOD1
HSP70
Soluble
Insoluble
Input
Actin
Spinal cord
h
Number of NeuN positive cells
Vehicle Amisodin
hTDP-43 (+/+)
j
Nucleus
Cytoplasm
Relative TDP-43 distribution (%)
Vehicle Amisodin
hTDP-43 (+/+)
l
Probability of Survival (%)
WT (Non-Tg) (n=6)
Vehicle (n=5)
Amisodin (n=3)
hTDP-43 (+/+)
9.7 days
Days

Fig. 5 Amisodin disrupts SOD1-TDP-43 proteotoxicity and reduces TDP-43 aggregation. **a, b** Amisodin suppressed cytoplasmic TDP-43 mislocalization induced by TDP-43 overexpression in SK-N-SH, NSC-34 and HEK-293T cells in a dose-dependent manner. Scale bar, 10 μm. The relative nuclear and cytoplasmic distribution of TDP-43 was quantified by cell counting, and the percentages are presented as mean ± SD (**b**). *$p < 0.05$, ***$p < 0.001$, ****$p < 0.0001$. **c** Amisodin blocked the interaction between SOD1-G147P and TDP-43. **d** Amisodin (5 μM) markedly reduced SOD1 and TDP-43 oligomerization induced by TDP-43 and/or SOD1-G147P overexpression. Mo (Monomer), Di (Dimer). **e** Amisodin did not affect the self-oligomerization of recombinant TDP-43 but markedly reduced the oligomerization of MT-SOD1 (G93A). **f** Schematic illustration of the experimental design for the analysis of offspring from Amisodin-treated hTDP-43 (+/-) parental mice. **g, h** Decreased NeuN levels in hTDP-43 (+/+) mice offspring (n=3) from vehicle-treated parents were significantly restored in offspring (n=2) from Amisodin-treated parents. Scale bar, 100 μm. The number of NeuN positive cells (red arrows) was counted (**h**). *$p < 0.05$. **i, j** Increased cytoplasmic TDP-43 in hTDP-43 (+/+) mice offspring (n=3) from vehicle treated parents was significantly attenuated in offspring (n=2) from Amisodin-treated parents. Red arrows indicated nuclear TDP-43 positive cells and blue arrows indicated cytoplasmic TDP-43 positive cells. Scale bar, 100 μm. The relative nuclear and cytoplasmic distribution of TDP-43 was quantified by cell counting, and the percentages are presented as mean ± SD (**j**). *$p < 0.05$. **k** Insoluble TDP-43 and mSOD1 accumulation in spinal cord lysates was reduced in hTDP-43 (+/+) offspring from Amisodin-treated parents compared with those from vehicle-treated parents. **l** hTDP-43 (+/+) offspring (n=3) from Amisodin-treated parents exhibited an approximately 9.7 days extension in lifespan compared with offspring (n=5) from vehicle-treated parents.

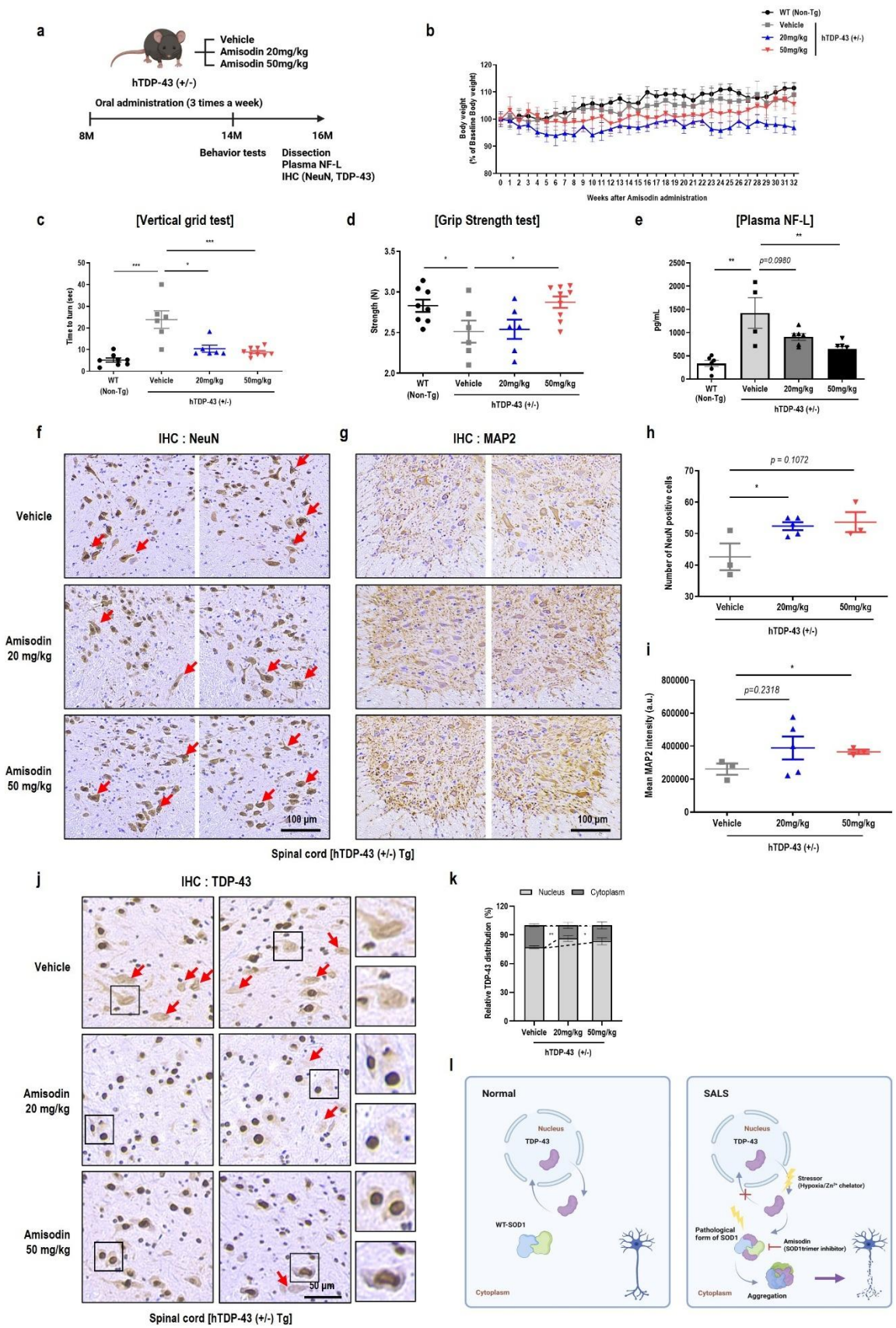

a
Vehicle
Amisodin 20mg/kg
Amisodin 50mg/kg
hTDP-43 (+/-)
Oral administration (3 times a week)
8M
14M
16M
Behavior tests
Dissection
Plasma NF-L
IHC (NeuN, TDP-43)
b
WT (Non-Tg)
Vehicle
20mg/kg
50mg/kg
hTDP-43 (+/-)
Body weight (% of Baseline Body weight)
Weeks after Amisodin administration
c
[Vertical grid test]
Time to turn (sec)
d
[Grip Strength test]
Strength (N)
e
[Plasma NF-L]
pg/mL
p=0.0980
f
IHC : NeuN
g
IHC : MAP2
Vehicle
Amisodin 20 mg/kg
Amisodin 50 mg/kg
100 μm
Spinal cord [hTDP-43 (+/-) Tg]
h
p = 0.1072
Number of NeuN positive cells
i
p=0.2318
Mean MAP2 intensity (a.u.)
j
IHC : TDP-43
50 μm
Spinal cord [hTDP-43 (+/-) Tg]
k
Nucleus
Cytoplasm
Relative TDP-43 distribution (%)
l
Normal
SALS
Nucleus
TDP-43
WT-SOD1
Cytoplasm
Stressor (Hypoxia/Zn2+ chelator)
Pathological form of SOD1
Amisodin (SOD1trimer inhibitor)
Aggregation

Fig. 6 Amisodin shows the therapeutic effect on the pathology of the hTDP-43 Tg mouse model. **a** Schematic illustration of the experimental design for oral Amisodin administration in 8-month-old hTDP-43 (+/-) mice. Mice received vehicle (n=6), Amisodin 20 mg/kg (n=6) or 50 mg/kg (n=9) three times per week. WT mice (n=8) served as controls. **b** No significant change in body weight was observed. **c, d** Amisodin treatment significantly improved motor performance in hTDP-43 (+/-) mice. Time to turn in the vertical grid test was reduced in Amisodin-treated mice (20 mg/kg, n=6, 50 mg/kg, n=8) compared with vehicle-treated hTDP-43 (+/-) mice (n=6) (**c**). Grip strength was improved in Amisodin-treated mice (20 mg/kg, n=6, 50 mg/kg, n=9) compared with vehicle-treated hTDP-43 (+/-) mice (n=6) (**d**). *$p < 0.05$, ***$p < 0.001$. **e** Amisodin significantly reduced plasma NF-L levels at 50 mg/kg (n=8). **$p < 0.01$. **f-i** Amisodin treatment showed the neuroprotective effect. Amisodin treatment increased both the number of NeuN-positive neurons (**f**) and MAP2 intensity (**g**) in the spinal cord. Scale bar, 100 μm. The number of NeuN positive neurons (red arrows) was counted (**h**). The intensity of MAP2 was quantified (**i**). *$p < 0.05$. **j, k** Amisodin treatment reduced the cytoplasmic TDP-43 mislocalization. Scale bar, 50 μm; enlarged images, 10 μm. The relative nuclear and cytoplasmic distribution of TDP-43 was quantified by cell counting, and the percentages are presented as mean ± SD (**k**). Red arrows indicated cytoplasmic TDP-43 positive cells. *$p < 0.05$, **$p < 0.01$. **l** Proposed model for SOD1-modulated TDP-43-associated pathology in sporadic ALS. Increased TDP-43 expression or cellular stress promotes its aberrant redistribution to the cytoplasm, where it interacts with pathogenic trimer-associated SOD1 conformers and facilitates SOD1/TDP-43 co-aggregation. Trimeric SOD1 acts as a pathogenic mediator linking TDP-43 mislocalization to reciprocal proteotoxicity. Pharmacological targeting of trimeric SOD1 by Amisodin attenuates the SOD1–TDP-43 interaction, thereby reducing aggregation of both proteins and ameliorating associated pathological processes. Created with BioRender.com.

Supplementary Files

This is a list of supplementary files associated with this preprint. Click to download.

- Additionalfile1.mp4
- SupplementaryFilesRawdatasets.pdf
- SupplementaryMethods.docx
- ExtendedDataFigure.pdf